THE UNIVERSITY OF MICHIGAN

INDUSTRY PROGRAM OF THE COLLEGE OF ENGINEERING

A STUDY OF THE DISLOCATION DISTRIBUTIONS IN ANNEALED 304 STAINLESS STEEL PRODUCED BY FATIGUE LOADING AT VARIOUS LEVELS OF STRAIN AND NUMBERS OF CYCLES

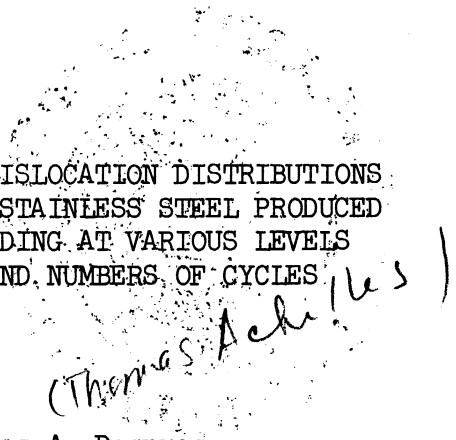

Thomas A. Despres

A dissertation submitted in partial fulfillment
of the requirements for the degree of
Doctor of Philosophy in the
University of Michigan
1963

September, 1963

IP-631

enm

UMR0568

ACKNOWLEDGMENTS

The author gratefully acknowledges all those who aided in this investigation and those associated with his doctoral studies, in particular the following:

Professor Julian R. Frederick, Chairman of the Doctoral Committee for his encouragement, counsel, and constructive criticism.

Professor W. C. Bigelow, Doctoral Committee member for advice, assistance, and invaluable discussions on specimen preparation techniques and use of the electron microscope.

Dr. Harry M. Bendler, Professors J. Datsko and D. K. Felbeck, members of the Doctoral Committee for their advice and assistance.

The Department of Mechanical Engineering for support of this study and for providing the author with financial support in the form of teaching fellowships.

Shell Oil Company, The Institute of Science and Technology, and The Ford Foundation for predoctoral fellowships and loans.

Dr. Robert Marcus, Mr. William Mitchell and Mr. Robert Little for their many helpful discussions of diffraction and fatigue theories.

Professors A. D. Moore and C. A. Siebert for their encouragement.

Dr. R. M. Fisher, and Mr. A. Szirmae for providing dimensions and photographs of their electropolishing apparatus.

The Staff of the Mechanical Engineering Machine Tool Laboratory for their cooperation in the fabrication of special tools and equipment.

All those who assisted in preparation of this manuscript.

TABLE OF CONTENTS

TABLE OF CONTENTS (CONT'D)

LIST OF TABLES

LIST OF FIGURES

LIST OF FIGURES (CONT'D)

LIST OF FIGURES (CONT'D)

LIST OF FIGURES (CONT'D)

INTRODUCTION

1. General

Fatigue in metals is one of the most important problems faced by engineers today. Numerous investigations of fatigue have been carried out for the purpose of (1) obtaining design data and parameters, or (2) obtaining information about the metallurgical variations and damage conditions resulting from fatigue. The ultimate aim of both types of studies has been to provide a basis for predicting fatigue lives and preventing fatigue failures under various service conditions.

Although the importance of obtaining design data and design parameters for prediction of failure and fatigue life cannot be overlooked, or even minimized, it does not suggest a means by which improvement of the fatigue properties of metals can logically result. Metallurgical studies, however, can lead to an understanding of the mechanisms involved. On the basis of an understanding of these mechanisms, materials with improved fatigue properties may eventually be evolved.

Before such improvements in materials can be made, it is necessary to know what characteristic conditions of damage are present in a metal during the process of fatigue. This necessary body of knowledge can be obtained by employment of various metallurgical techniques of observation during and after the fatigue process. The most promising tool which is presently available for these studies is the electron microscope. For some time now it has played a very important role in the identification of metallurgical structures and in the understanding

of their relation to the mechanical properties of metals. More recently, specimen preparation techniques have been developed which allow the electron microscope to be used for direct observation of dislocations in metals. This latter development has many advantages in the study of metals and can be applied to study the dislocation distributions resulting from the fatigue process.

2. Problem Statement

This investigation has been undertaken in order to obtain and compare information about the dislocation distributions present in an annealed commercial 304 stainless steel sheet as a result of the following conditions of mechanical deformation:

1. pure tension at strain levels above the proportional limit.
2. constant amplitude cyclic loading at strain levels near the yield strain, and at various numbers of cycles.

3. Selection of Material

Type 304 stainless steel is a face-centered cubic alloy of low stacking fault energy which has many engineering applications. Whereas excellent work has been done in transmission electron microscopic studies of fatigued 304 stainless steel by previous workers,[33], [48] their objectives did not require variation of the stress level or the number of cycles; consequently, information regarding the influence of these important variables on the dislocation distributions is not available. Such information is essential for understanding the mechanism of fatigue failure.

4. Selection of the Method of Fatigue Loading

The selection of the method by which a specimen is fatigued is influenced by the desired strain level. For low cycle fatigue, constant strain results are more meaningful than constant stress results since the deformation is not dependent upon the cyclic hardening characteristics of the material. Also, the strain is not dependent upon the inertia of the fatigue machine.

The interest in fatigue is generally in the condition of zero mean stress since this condition of loading is usually attained in practice. Although it is extremely difficult to maintain zero mean stress in thin fatigue specimens, it is easier to approach this condition using deformation by reversed bending than by using push-pull, tension compression deformation. For these reasons, reversed bending at constant strain was selected for this work. This selection also provides a basis for comparing the results with the results of other work.

The problems involved in preparation of the specimens for examination by transmission electron microscopy often place a practical limitation on the size of the test specimens. For this reason, many test specimens which have been used for electron transmission studies were thin sheet with thicknesses of 0.002 to 0.015 inch. These thicknesses, however, may not be representative of the bulk condition of the material or of the mechanical deformation process. If thick specimens are fatigued in reversed bending, it is relatively easy to maintain zero mean stress. Therefore, it is necessary to use a specimen that is thick enough to maintain zero mean stress easily and still thin enough so that preparation

of the specimens for examination by electron transmission microscopy is feasible. The use of 1/16 inch thick specimens provides a satisfactory compromise that is (1) representative of the bulk condition of the material and the process of mechanical fatigue, (2) thick enough to maintain zero mean stress, and (3) thin enough to make electron transmission specimen preparation practical.

REVIEW OF THE LITERATURE

1. General

In 1903, Ewing and Humfrey[11] presented some of the first work on the study of microstructural changes in metals resulting from fatigue loading. With this work, they advanced their "attrition theory" of metal fatigue based on the observations of slip line formation in metals and the "expulsion of debris" (now commonly referred to as the "formation of extrusions") at or near the slip lines. From this time until 1924, no significant advances were made in the understanding of fatigue. Although the literature of that period contains many theories on the mechanism of fatigue, these theories were modifications of Ewing and Humfrey's attrition theory.

Beginning in about 1924, Gough and his co-workers[18]-[23] reported on a series of fundamental studies that form the basis for much of the present knowledge of fatigue. In particular, they were among the first to use single crystal fatigue specimens to achieve an accurate relation of the fatigue deformation to crystal structure, and were able to show the directional movement of slip during fatigue to be on the $\{111\}$ planes and in the $\langle 110 \rangle$ directions for face-centered cubic crystals. They also showed the effects of atmosphere on the fatigue process, and concluded that fatigue crack propagation is dependent on environmental conditions, but that fatigue crack initiation is not.[21]-[23] These latter conclusions have since been confirmed by Wadsworth and Hutchings.[64]

One of the more interesting results of fatigue loading is the formation of slip bands. Metallographic studies of slip band formation

have been made on steel by Hempel and co-workers[27],[28] and on aluminum by Forsyth[14],[15] using light microscopy techniques. Thompson[59] employed the electron microscope and surface replica techniques to study the slip band phenomenon. He observed "persistent" or "uninhibited" slip bands which first appeared after very few cycles. Kemsley,[41],[42] also found persistent slip bands, but only at low stress levels. Wood[77]-[80] hypothesized that there are two types of slip caused by fatigue; fine and coarse. He referred to coarse slip as fatigue banding and suggested that two fatigue mechanisms occur, one at low stress levels and another at high stress levels. Bendler and Wood[6],[7] employed replica and taper sectioning techniques to study banding, intrusion, and extrusion in oxygen-free, high conductivity copper by light and electron microscopy. Based on these types of observations of slip bands, it has been proposed that fatigue cracks result from voids left behind by extrusions[44] or from the growth of intrusions.[10]

2. Transmission Studies of Fatigue

At present, the literature contains only a limited number of articles describing transmission electron microscopic studies of fatigue, and most of these involve metals having face-centered cubic lattice structures.

Hirsch, Partridge, and Segall[33] attempted to show the relation between surface slip steps and dislocation arrangements below the surface. Fatigue specimens of 0.012 inch sheet 18/8 stainless steel were fatigued in reversed bending at very low stresses giving fatigue lives on the order of 10^8 cycles. The thin films for examination by transmission

microscopy were prepared by electropolishing the fatigued samples from one side only, using a modification of the Bollman technique[9] which was developed by Tomlinson.[60] They concluded that the dislocation distribution at the surface is similar to that below the surface.

Segall and Partridge[49] used transmission electron microscopy to study foils prepared from 1/16 inch aluminum sheet that was fatigued in reversed bending. They concluded from their observations that the subgrain size which results from fatigue at high stress levels is larger than the subgrain size that results from unidirectional tensile deformation. They observed that a lower density of dislocations was present within the subgrains of aluminum deformed in unidirectional tension. Polygonization, similar to that observed in unidirectional tension at high plastic strains, was present in the foils prepared from the fatigued specimens. Aluminum fatigued at low stresses showed an extremely high density of stable dislocation loops very similar to the stable dislocation loops found in quenched aluminum, although the dislocation loops in the fatigued material were present in regions of high dislocation density while those present in the quenched specimens were usually uniformly distributed except near the grain boundaries where they were very few in number.

Build-up of subgrains under push-pull, tension-compression fatigue was found for fatigued aluminum by Wilson and Forsyth,[76] by Grosskreutz,[24],[25] and by Grosskreutz and Waldow.[26] In the work of these last authors, using flat strips 0.005 inch thick of polycrystalline annealed aluminum cemented to plastic bars 0.025 inch thick and then

fatigued by reversed bending at constant amplitude, distinct subgrains were observed after 500 cycles. This is in contrast to the results of Segall and Partridge[49] who did not find subgrain formation in specimens of aluminum that were fatigued by constant reversed stress for the same fatigue lives.

Segall, Partridge and Hirsch[48] studied fatigued specimens of various single crystal and polycrystal face-centered cubic metals. Copper, nickel, gold and a specimen of 18/8 stainless steel deformed by reversed bending at high constant stress (50,000 cycle life) were all found to form the same type of dislocation arrangements. Dislocations and dislocation loops were generally concentrated in localized regions separated by regions of approximately the same width having a very low density of dislocations. They pointed out that for these materials the dislocation distribution that resulted from fatigue at high stresses differed from that produced by unidirectional tension in that no cellular structure is formed by fatigue and that most of the dislocations that existed after fatigue are in the form of loops. They concluded from their results that the distributions of dislocations 100 microns below the surface are similar to those at the surface.

Snowden[50],[51] attempted to correlate cyclic hardening with dislocation arrangement in single crystal aluminum oriented for single slip. His results for specimens strained in the easy glide range in completely reversed tension and compression suggested that the presence of dislocation tangles has an important influence on the Bauschinger effect and the cyclic hardening of crystals. He also suggested that the formation of tangles is likely to be an irreversible process and that they may act as obstacles to disloca-

tion motion as well as dislocation sources. This notion is in agreement with the work of Wilsdorf and co-workers.[69],[70],[72],[75]

3. Dislocation Tangles and Cellular Structure

Experimental evidence[17],[48] suggests that for unidirectional tension, initially isolated tangles increase in number and gradually develop into a cellular structure of dense tangles surrounding regions of low dislocation density. This cellular arrangement of dislocation tangles has been observed in bulk pure materials deformed unidirectionally at relatively high strains, and has also been found in fatigued specimens of pure metals having high stacking fault energy.[12],[48],[49] Dense tangles forming cellular structure have not been reported for brass or other materials having low stacking fault energy under either unidirectional tension or fatigue loading. Theories relating the appearance of tangles to point defects, old and new dislocations, and vacancy clusters are discussed by Wilsdorf, Maddin and D. Kuhlman Wilsdorf.[73]

4. Transmission Studies of Stainless Steel

In addition to the studies conducted on specimens from fatigued specimens, a number of other transmission electron microscopic studies of dislocations and dislocation interactions have been carried out using stainless steel because of its low stacking fault energy and the characteristic dislocation pile-ups found in it. Whelan, Hirsch, Horne and Bollman[67] examined thin foils (.007-008 inch thick) of 304 stainless sheet cold rolled to achieve different amounts of cold work up to 10 per cent reduction in thickness. Their results showed that the dislocation arrangements had an

increasing departure from simple dislocation pile-ups as the amount of cold reduction increased. Hexagonal dislocation networks were observed after approximately 2.5 per cent strain. With a slightly greater amount of strain, irregular networks of dislocations were reported to be prominent, and dislocation densities near grain boundaries were reported as being considerably higher than in the interiors of the grains, although no micrographs of specimens strained above 2.5 per cent were shown. Several dislocation interactions in stainless steel have been treated theoretically by Whelan.[65] H. G. F. Wilsdorf and D. Kuhlman Wilsdorf[70] have studied the behavior of dislocations and dislocation loops in quenched and in irradiated stainless steel. In none of these studies were cellular distributions of dislocation tangles reported. The maximum thickness of the material used in these studies was 0.012 inch.

EXPERIMENTAL PROCEDURE

1. Material

The material used in this study was 1/16 inch commerical 304 stainless steel sheet with the composition:

Cr	Ni	C	Mn	Mo	Si	Cu	P	S
18.10	9.25	0.077	0.94	0.21	0.47	0.22	0.021	0.023

The annealed grain size was A.S.T.M. 5-7, and the grains had a preferred orientation of the < 110 > direction normal to the surface from previous processing. The tensile properties of the annealed sheet material prior to fatigue or tensile deformation were:

Yield Strength = 29,000 P.S.I.

Tensile Strength = 80,000 P.S.I.

Young's Modulus = 30×10^6 P.S.I.

Reduction in Area = 59 per cent

A stress-strain curve of the material for low strains is plotted in Figure 1.

2. Preparation of the Fatigue and Tensile Specimens

The fatigue specimens were of the constant strain type as shown in Figure 2. The tensile specimens were of the standard sheet tensile type with a gage length of 2-1/2 inches and a cross sectional area of .060 square inches.

After machining, the fatigue and tensile specimens were annealed at 1900-1950°F for one hour, water quenched and then heated to 400°F to relieve stresses. No appreciable precipitate was observed

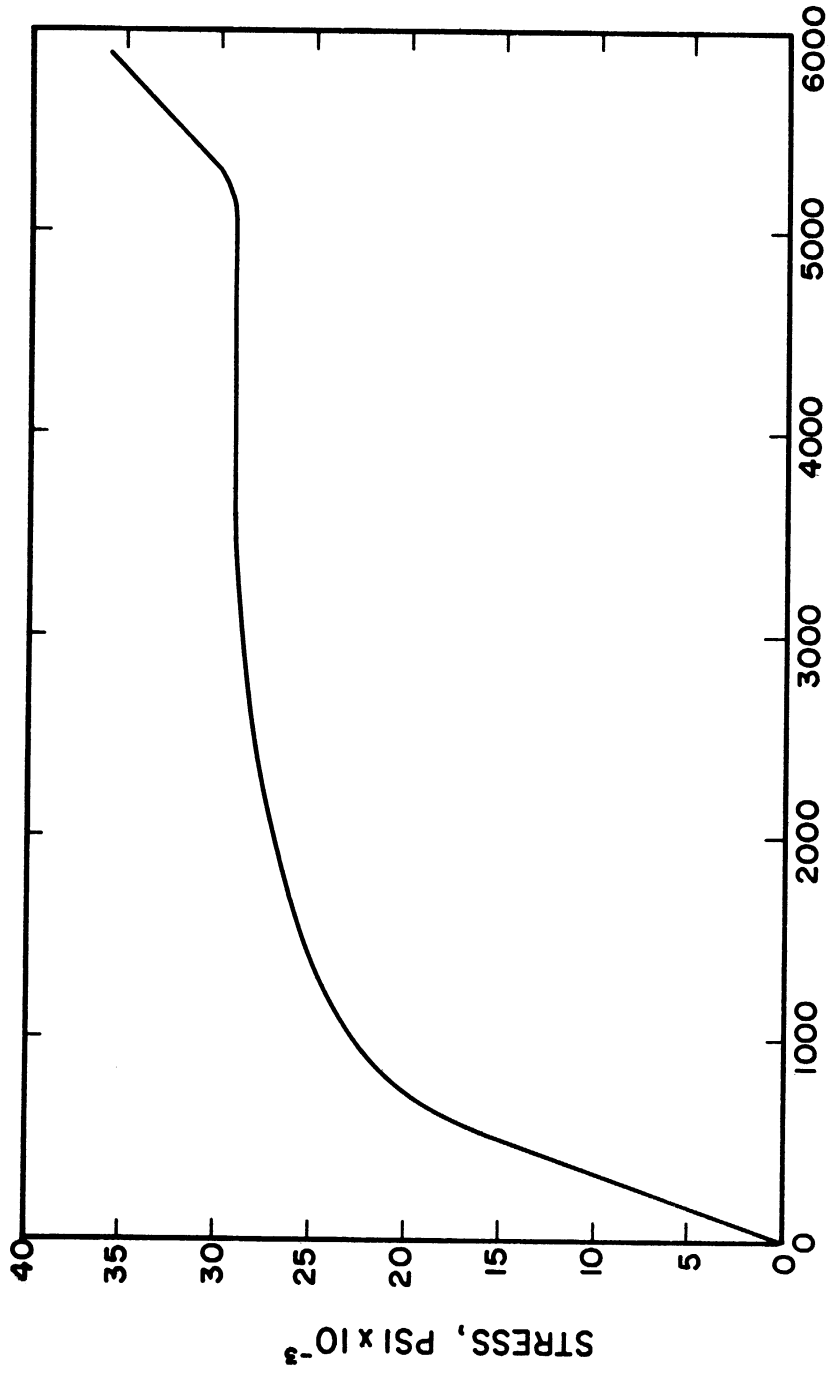

Figure 1. Stress-Strain Curve for Low Strains.

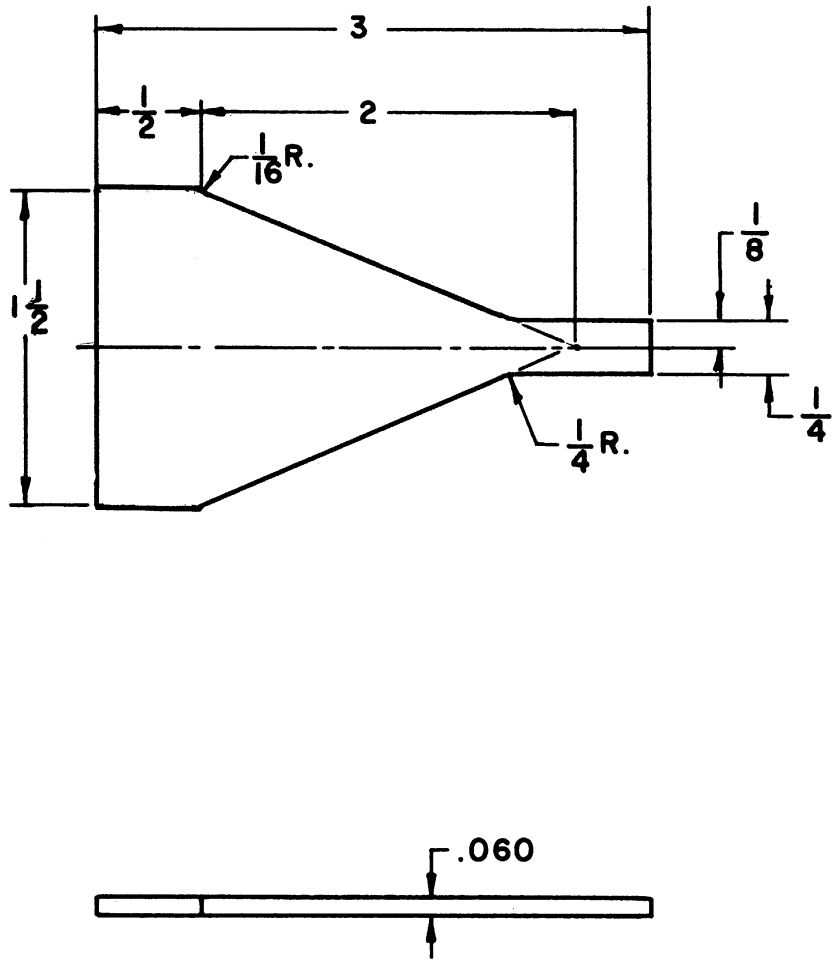

Figure 2. Dimension Drawing of the Fatigue Specimen.

in the specimens. After the heat treatment, one surface of the fatigue specimens was mechanically polished through 1/4 micron diamond grit and then electropolished to remove approximately 0.001 inch of metal from the polished surface to assure elimination of surface damage from the mechanical polishing.

3. Fatigue Testing

The fatigue tests were conducted by reversed bending using the constant amplitude fatigue machine shown in Figure 3. This machine incorporates use of a specimen cradle to minimize superimposed horizontal tension during bend cycling. The numbers of cycles and the levels of strain used in the various tests are listed in Table I.

TABLE I

STRAIN LEVELS AND CYCLES OF FATIGUE

Strain	Number of Cycles				
1050					$5.5 \times 10^{6*}$
1600	5×10^{3}	1×10^{5}	5.5×10^{5}		$1.0 \times 10^{6+}$
3000	5×10^{3}	$85 \times 10^{3+}$			
5650	10	50*	200*	1000*	11,000+

*Foils were obtained from the surface.
+Failure occurred at this number of cycles.

4. Tensile Testing

The tensile specimens were deformed in a Tinius-Olsen 60,000 pound capacity tensile machine. The unidirectional strains to which the specimens were deformed are listed in Table II. Deformations less than one per cent were measured by means of a Pico visual

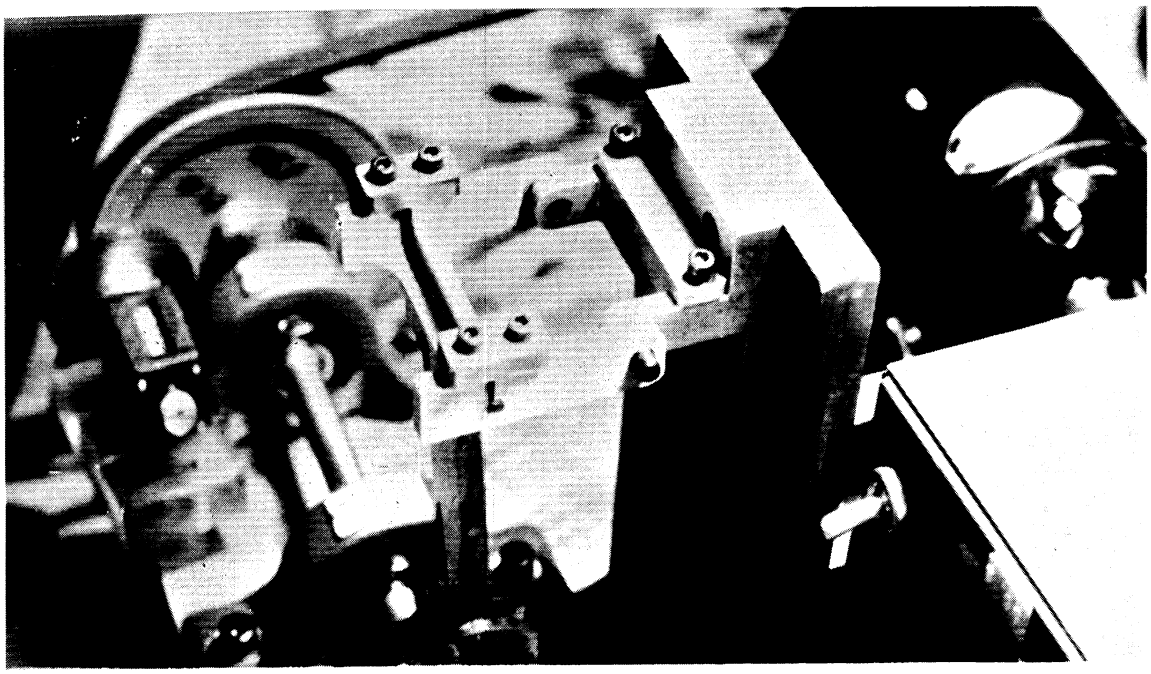

Figure 3. Constant Amplitude Fatigue Machine.

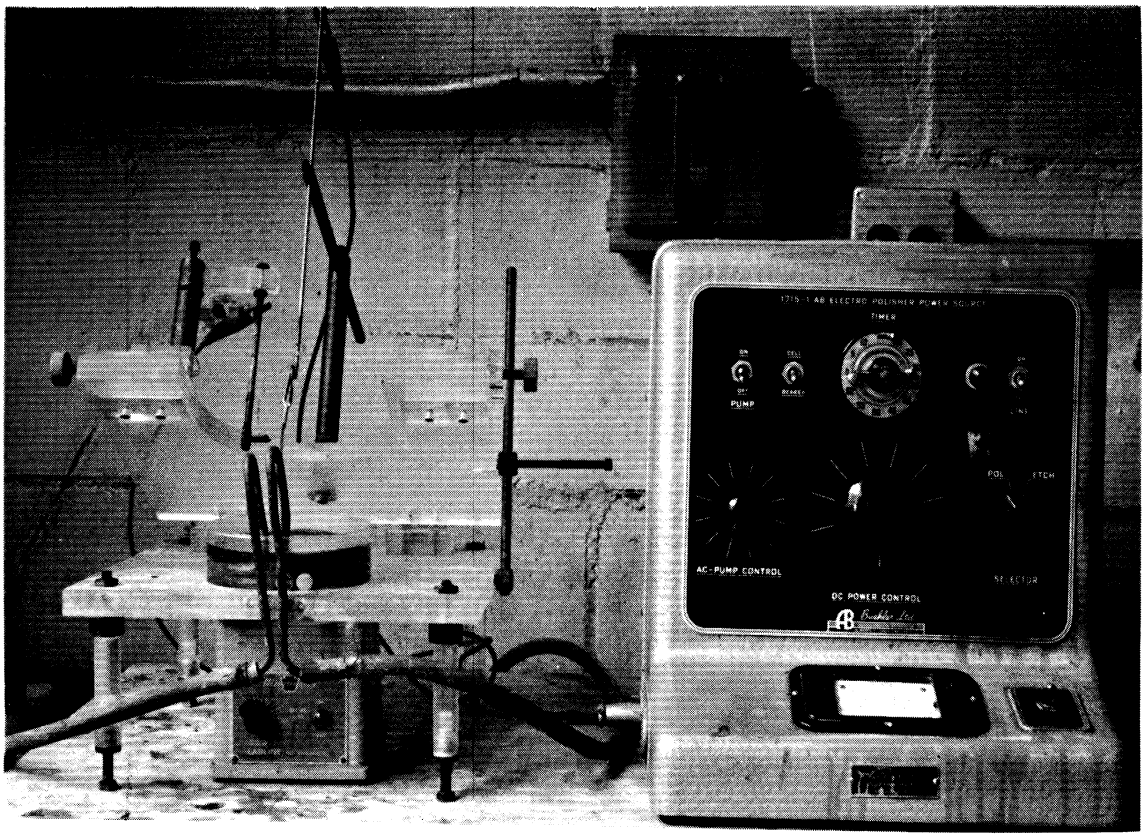

Figure 4. Electropolishing Apparatus Used for the Second Step of the Thinning Process. On the left is the Fisher-Szirmae apparatus. Adjustment of the cathode is made through movement of the cross slide. Tap water passes through the coil which is immersed in the electrolyte thereby cooling the electrolyte.

strain indicator which was connected to an Alinco foil strain gage. The strain gages were bonded to the tensile specimens with Eastman 910 contact cement. Calipers were used to determine the magnitude of the higher strains.

TABLE II

LIST OF TENSILE TESTS

TEST NO.	STRAIN
1	3,000 Micro-inch/inch
2	5,650 Micro-inch/inch
3	10,000 Micro-inch/inch
4	5.0 Per cent
5	10.0 Per cent
6	20.0 Per cent
7	Fracture

5. Preparation of Thin Films for Electron Transmission Examination

After the fatigue and tensile specimens were strained, pieces of metal approximately 5/8" by 5/8" were cut from them with a fine blade hacksaw and thinned to the thickness required for electron transmission examination. Thinning of the specimens from the original thickness was done in a three steps; the first was mechanical, and the following two were electrolytic polishing. The thinning of the fatigue specimens was done from one side so that the final films for examination in the electron microscope could be taken from the metal at the polished surface or from the metal within .0015 inch of the polished surface. The tensile specimens were thinned so that films were taken from the region of the neutral axis.

a. Fatigue Specimens

The first thinning step consisted of wet polishing the specimens through the following metallographic papers to a thickness in the range of 0.012 inch to 0.018 inch. The approximate thickness at which polishing was stopped for each metallographic paper was:

100 grit: 0.020 to 0.025 inch.

240 grit: 0.016 to 0.022 inch.

400 grit: 0.014 to 0.020 inch.

600 grit: 0.012 to 0.018 inch.

During the first thinning step the specimens were glued to a 1" x 2" x 3/4" steel block so that they could be manipulated easily. Eastman 910 contact cement was found to be a satisfactory agent for fastening the specimen to the steel block because, in addition to its relatively high bonding strength, it hardens rapidly, bonds uniformly over the contact surface, and is insoluble in water but dissolves easily in acetone. The uniform bond was necessary to eliminate buckling of the specimens and to provide a base from which the specimens could be evenly referenced during the mechanical polishing. The insolubility in water permitted the use of wet polishing procedures to minimize surface heating while the easy solubility in acetone allowed the specimen to be removed from the steel block after polishing without thermal, mechanical or chemical damage.

The second thinning step consisted of electropolishing the specimens from one or both sides to a thickness of less than .001 inch. Electropolishing was done in an electrolyte of 60 per cent orthophosphoric and 40 per cent sulphuric acid at room temperature and a D.C. voltage of

6-9 volts, using the Fisher-Szirmae apparatus shown in Figure 4. This apparatus provides independent control of cathode location and anode location. This feature is necessary since adjustments of the cathode location with respect to the specimen must be made as the electropolishing progresses. In addition, the cathode and the anode can be rapidly removed from the electrolyte, thereby terminating the electropolishing and minimizing possible etching of the specimen. The objective of this step was to obtain as large a piece of the specimen as possible having a uniform thickness less than 0.001 inch.

A procedure was found to be effective in reaching this objective. With the relatively thick specimens a more uniform thinning was obtained when only one face and the four thin sides (0.012 - 0.016 inch thick) of the specimen were completely masked with Microstop* during the electropolishing. Whenever preferential thinning at the specimen edge became visibly apparent during electropolishing the process was stopped and the mask was dissolved in acetone. The mask was then renewed over the same area as before and the electropolishing was continued.

This process was continued until the specimen was less than 0.003 inch thick, except for the case where the foils were being prepared from metal at the surface of the specimen. In this case the electropolishing was continued from one side to less than 0.001 inch. The 0.003 inch material was then electropolished from both sides until the specimens were less than 0.001 inch thick. It was necessary to mask the edges of the specimen to minimize preferential thinning there.

*Microstop is an acetone base, non-conducting lacquer manufactured by Detroit Chrome and Chemical, Detroit, Michigan.

The third step in the preparation of the foil consisted of electropolishing the thin piece of the specimen prepared by the above two steps from one or both sides to the thickness required for electron transmission examination. The method employed for this step basically consisted of electropolishing the material held between two relatively thin washers as shown in Figure 6. The washers formed a rigid support frame which provided ease in handling and storing the specimen assembly. Final handling operations were performed in the protection of this support frame. The geometry of the specimen assembly was chosen such that the assembly could be placed directly into the standard specimen holders of the microscope. The washers also form a conducting mask around the foil edges which acts to provide a uniform current density over the surface of the foil.

The assembly was joinned by spotwelding the washers together at the locations indicated by the crosses in Figure 6 while the assembly was held in the forceps shown in Figure 5. The forceps provided a jig for assembling the washer-foil sandwich and also provided a means of holding the assembly without damaging it during the spotwelding operation.

The area of thin metal that resulted from the second thinning step was usually about 1/4 inch^2. This area was cut into 0.1 inch squares by either of two methods. In the first method a scalpel was used to cut the squares directly from the thin metal while a smooth piece of plexiglass was used as a cutting base. The second method employed preferential electropolishing to cut out the small squares. In this method the small squares were obtained by lacquering a grid

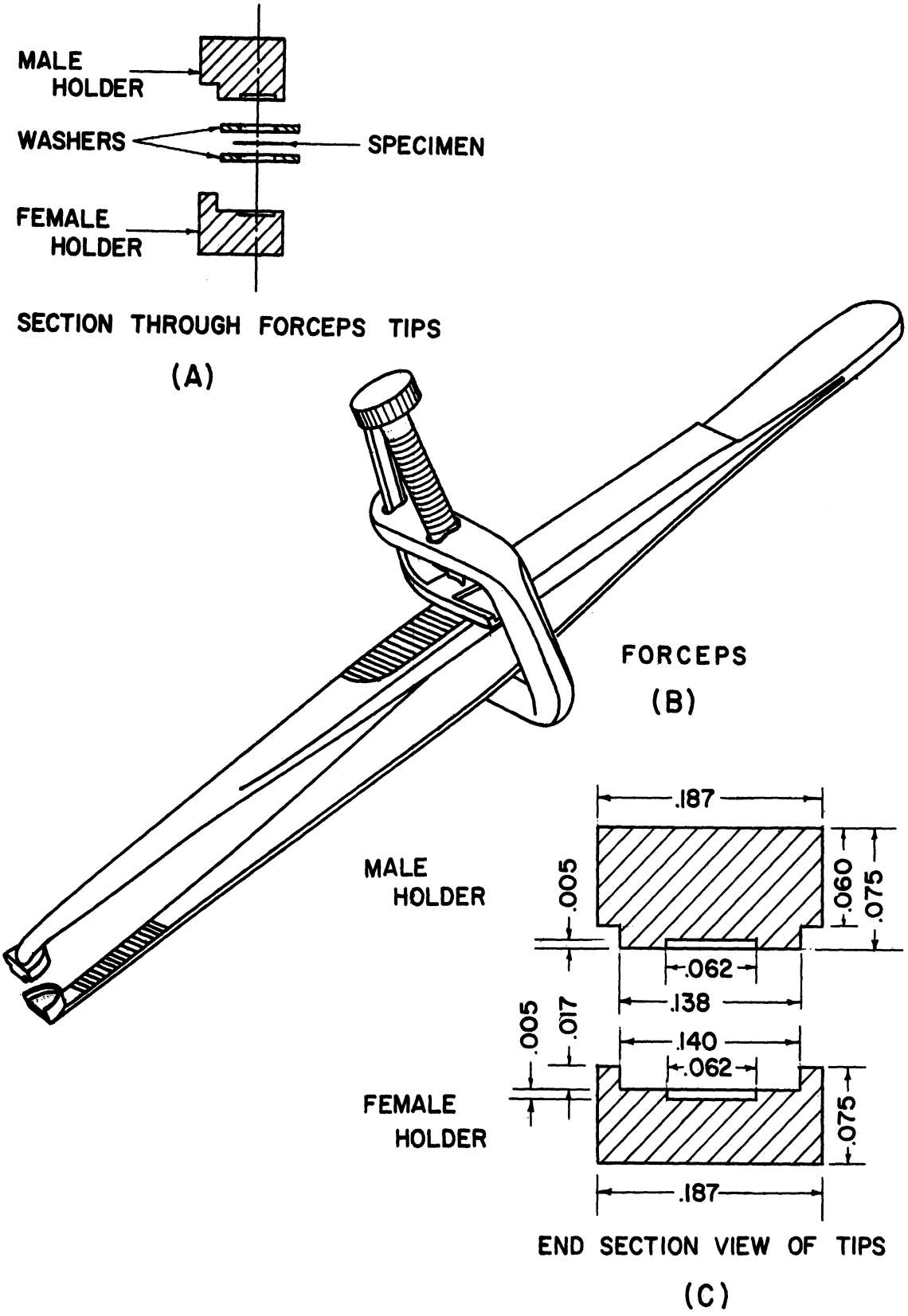

Figure 5. Forceps Employed for Holding the Specimen Assembly During Spotwelding.

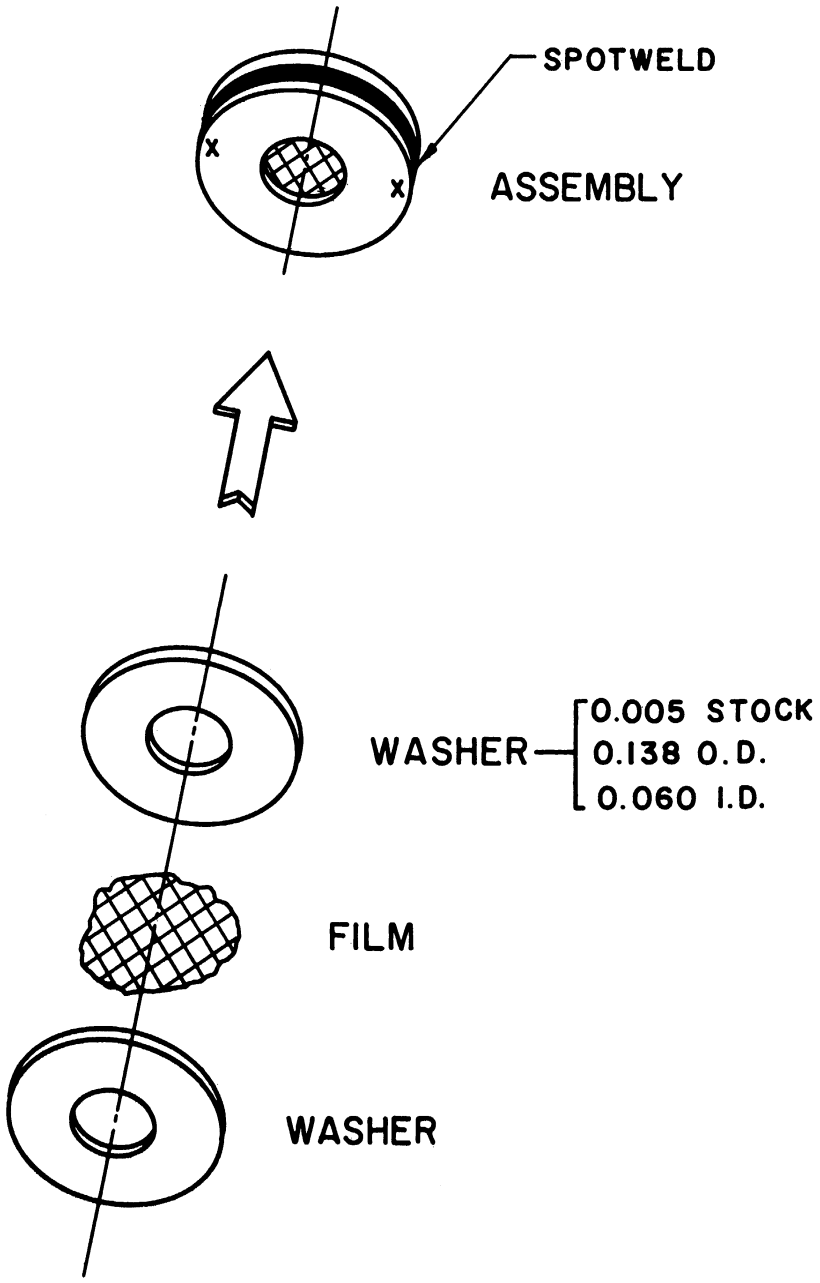

Figure 6. Sketch Showing the Assembly of the Specimen Prior to the Third Step of the Thinning Procedure.

of 0.1 inch squares on one side of the thin foil and then further electropolishing the foil until preferential thinning at the lacquer edge dissolved the metal that was exposed from both sides. Several 0.1 inch squares usually were obtained from each specimen and joined between the washers immediately after the second thinning step. They were then stored in a desiccator until electron transmission microscopy studies were made of them.

The final electropolishing was done in the manner illustrated in Figure 7. The forceps shown here acted as the anode lead and are insulated except at the tips where they make electrical contact with the specimen assembly. The electrolyte mixture was held in a small glass or a beaker in which a cathode was placed. The geometry of the cathode did not appear to have any effect on the uniformity obtained in the foils. The electrolyte and voltage used for this step was the same as that used for the second thinning operation, i.e., 60 per cent orthophosphoric - 40 per cent sulphuric acid and 6-9 volts D.C. The electropolishing was arrested when a small hole appeared in the foil. Usually the foil thinned in this manner would contain relatively large areas which were suitable for electron transmission microscopic examination. If the thin areas were not sufficiently large when examined in the microscope, the specimen was removed from the microscope and electropolishing was continued until the foil contained suitable areas. After electropolishing was stopped, the foil was immediately washed in distilled water and then air dried. Excess water was blotted off the washers with lens tissue or bibulous paper.

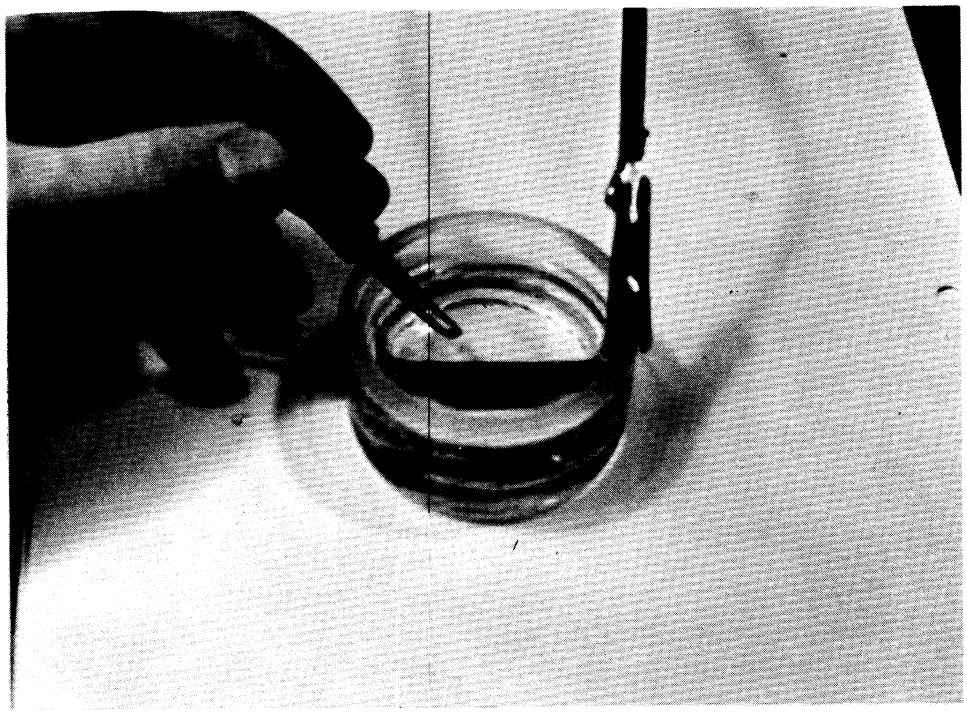

Figure 7. Photograph Showing the Final Thinning Operation. The forceps act as the anode lead and are covered with a nonconducting mask except at the tips where electrical contact is made with the specimen assembly. The cathode is shown immersed in the electrolyte.

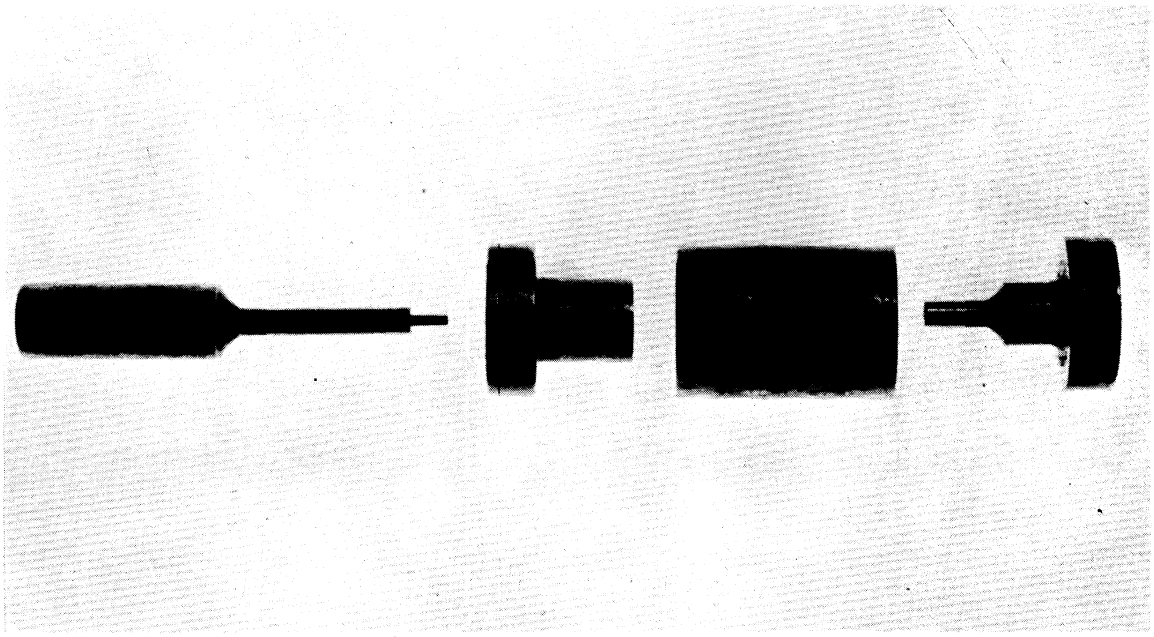

Figure 8. Combination Punch and Die Used for Making the Washers for the Specimen Assembly.

The washers used were made from 304 stainless steel. This material was selected because of its favorable welding and magnetic characteristics. The washers were made by the combination punch and die shown in Figure 8.

b. Tensile Specimens

In order to obtain the films from the neutral axis of the tensile specimens a slight variation in procedure was required. The specimens were mechanically thinned to 0.038 inch thick in the same manner as the fatigue specimens and removed from the steel blocks. The specimen was then glued to the block with the unpolished side up and thinned mechanically to approximately 0.015 inch to 0.018 inch. After the mechanical thinning, electropolishing was conducted from one side only until the specimen was approximately 0.009 inch thick. At this thickness electropolishing was conducted from the other side until the metal was approximately 0.003 inch thick. When the specimen metal was approximately 0.003 inch thick, thinning was continued from both sides to less than 0.001 inch thick. The procedure for the final thinning was the same as for the fatigue specimens.

Transmission Studies

The electron transmission studies were conducted at 80 and 100 K.V. on a J.E.M. Model 6A electron microscope equipped with a tilting attachment. A minimum of five films and in some cases as many as 15 were examined for each condition of fatigue. For certain conditions of fatigue,* electron transmission observations were made

*Marked with an asterisk in Table I.

from foils that were obtained from within 0.3 microns of the fatigue specimen surface.

A tilting stage with an angular range of $\pm 20^{\circ}$ was employed to obtain optimum reflection conditions and to determine the effect of varying reflections on the observed images. Although the tilting attachment was not used on all foils it was used on several foils from each fatigue specimen.

OBSERVATIONS

1. Dislocation Rearrangement During Electropolishing

The structures that are observed in thin metal foils by transmission electron microscopy may be different from those which were present in the thick specimens from which the foils were prepared because handling and electropolishing can cause rearrangement of the dislocations in the foils. In the present study, the rigid support provided by the washers minimized dislocation rearrangement during handling of the thin foils. A loss of dislocations from the surface of the specimen has been found to result during electropolishing.[61],[62],[75] For this reason there is a minimum thickness at which the foils should be examined in order to obtain results that are representative of the structure of the thick specimens. This loss of dislocations was also apparent in the present study. For example, the thinner regions of the metal near a hole in the foil often would have the same appearance as thicker regions in an annealed foil. As the thickness increased away from the edge of the hole, there was a corresponding increase in the dislocation density until a certain thickness was reached at which the arrangement of dislocations appeared to be the same as in the thicker regions of the foil. Unfortunately, there are no known means available by which rearrangement and loss can be controlled during electropolishing. However, the problem of rearrangement and loss during electropolishing was minimized in this study by making observations only on the thicker portions of the foil. The solutions used in this study to minimize dislocation rearrangement appear to be the best available at the present state of the art.

2. Effect of Surface Preparation and Mechanical Thinning

Work was undertaken to determine if (1) preparation of the surface of the fatigue specimens and (2) mechanical thinning of the specimen to .012 - .018 inch caused damage to the surface and to the regions from which the thin films were taken. A specimen of annealed stainless steel was subjected to the same techniques of surface preparation and film preparation as the fatigue test specimens except that it was mechanically thinned to 0.006 inch thick prior to electropolishing. Areas from foils of this annealed and thinned specimen are shown in the micrographs of Figures 9 and 10. By tilting the foils in the electron microscope the specimen was found to have a relatively low density of dislocations. Figure 10 shows a specimen tilted to show the maximum number of dislocations and their random orientation and nature. From the observations made on these foils it was concluded that damage caused by surface preparation or by mechanical thinning was negligible. Support for this conclusion was found in the observations made from the foils of specimens strained at very low tensile strain. Figure 11 and 12 are electron transmission micrographs from these foils. The dislocation distributions were similar to those obtained by Whelan[65] and Hirsch[30] for the same strain levels. In their work initially thin annealed stainless steel sheet was rolled various amounts and then electropolished using the Bollman Technique[9] to prepare the thin foils. Since the results were essentially the same for the two methods, it was concluded that the first thinning step does not damage the foil. The work of Szirmae and Fisher[54] can also be used to support the use of the first step of thinning. Their work showed that there was very little difference

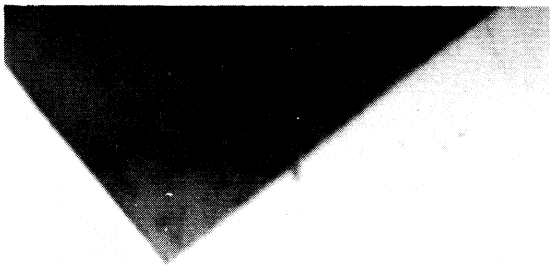

Figure 9. Transmission Micrograph of a Thin Foil Prepared from the Surface of an Annealed Specimen of 304 Stainless Steel. 14,000X

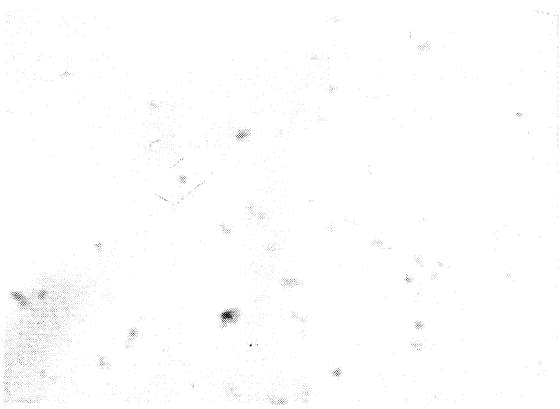

Figure 10. Transmission Micrograph of a Thin Foil Prepared from the Surface of an Annealed Specimen of 304 Stainless Steel. A region of high dislocation density. 10,000X

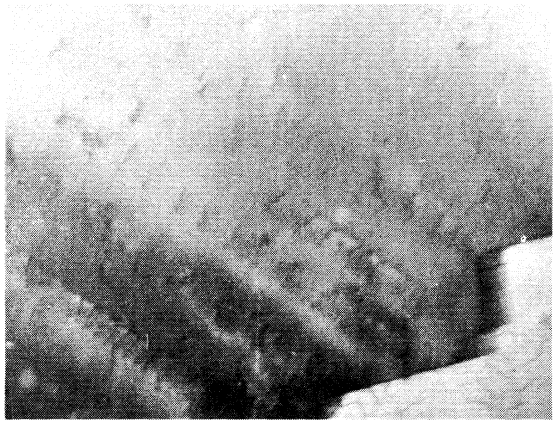

Figure 11. Transmission Micrograph Showing Dislocation Pile-ups Resulting from an Unidirectional Tensile Strain of 0.3 Percent. 8,000X

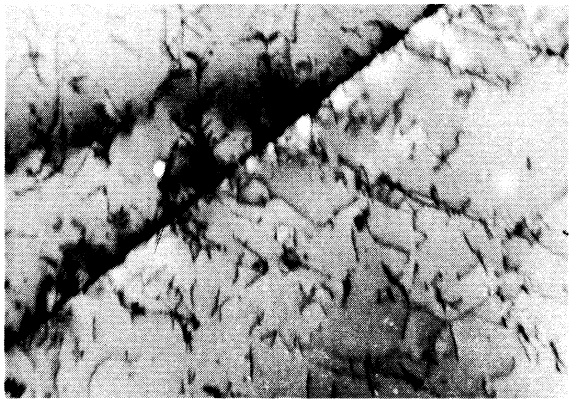

Figure 12. Pile-ups and Interaction of Pile-ups on Different Slip Systems Near a Grain Boundary. Micrograph obtained from a specimen that was deformed 0.56 percent by unidirectional tension. 6,100X

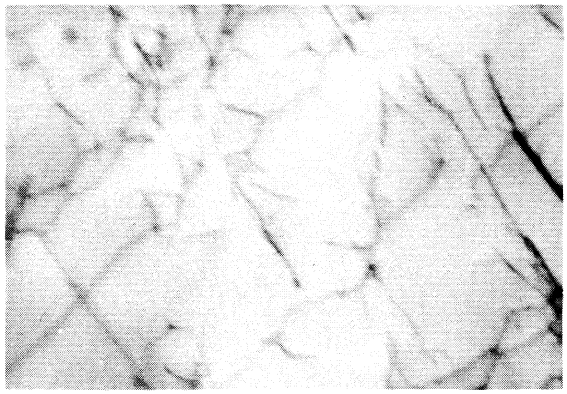

Figure 13. Formation of Regular and Irregular Networks Caused by a Unidirectional Tensile Strain of 0.56 Percent. 18,000X

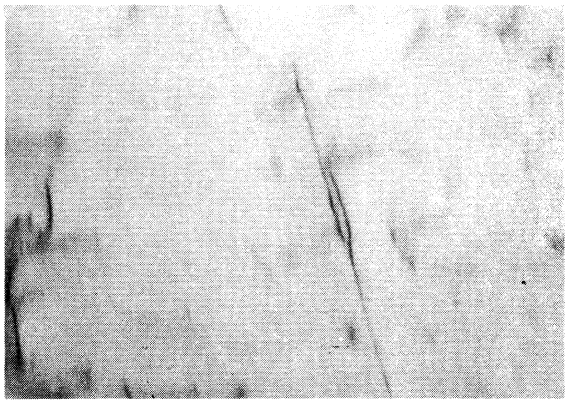

Figure 14. Dislocation Interactions at One Percent Unidirectional Tensile Strain. 18,000X

in the dislocation density and the dislocation distributions present in a foil that had only been thinned by electropolishing and those present in a foil obtained by electropolishing after mechanically thinning to 0.002 inch by sanding with 500 grit metallographic paper.

3. Results from Specimens Deformed in Tension

The dislocation distributions observed as a result of increased deformation in tension on the 1/16 inch thick specimens of 304 stainless steel support the observations of previous workers[65],[67],[48] on 0.1 and 0.2 mm. stainless steel foil. A definite variation of dislocation arrangements occurred which apparently paralleled the inflection points of the nominal stress strain curve of this material. The stress-strain curve of this particular material has a definite "hold" above its proportional limit as shown in Figure 1. This hold starts at approximately 1000 micro-inch/inch strain and persists to 5000 micro-inch/inch strain. Coinciding with this flat portion of the curve were dislocation arrangements of the type shown in Figures 11 and 12. At the low end (.1 per cent strain) simple pile-ups of dislocations were observed at the grain boundaries and were primarily present on one slip system of each grain. At the higher (.3 - .5 per cent strain) end of this hold, dislocation pile-ups were present on different slip systems and interactions of these pile-ups were predominant throughout the grains. The densities of pile-ups and of isolated dislocations were not uniform throughout all grains.

At slightly higher strains, the stress-strain curve rises sharply. At one per cent strain, dislocation interactions became more

numerous, and regular as well as irregular dislocation networks resulted. These networks were found to increase in density and irregularity with increasing strain to above five per cent. Figures 13 through 17 show dislocation interactions and irregular networks in the specimens strained at one per cent and five per cent. At 10 per cent strain the first cell structure on dense dislocation tangles was observed. Figures 18 and 19 show the cell structure of dense dislocation tangles which resulted from strains of 10 per cent and 20 per cent respectively. These tangles were not predominant throughout the material but were definite and dense within certain grains. In this approximate range of strain the slope of the nominal stress-strain curve starts to decrease. At higher strains there was a greater density of cell structure of dislocation tangles and large regions of faulted material as are shown in Figures 20 and 21. At fracture, which corresponds to a true strain of 0.9, extremely dense cells resulted. They were, however, not prominent but were rather intermittently dispersed throughout the material. Two other more prominent features were observed in these films. One of these was an extremely faulted structure of which Figure 21 is a typical region. The second prominent feature was the interaction of stacking faults which were present within different planes.

These results show a definite characteristic relation between portions of the stress-strain curve and the defect structure of stainless steel as observed by electron transmission microscopy. In the flat portion of the curve, apparently dislocations were able to glide easily and form the simple pile-ups which increase in density and number of dislocations with little increase in flow stress. The termination of this portion of the curve appeared to coincide with longer range interactions of dislocations

Figure 15. Regular and Irregular Networks Produced by Five Percent Unidirectional Tensile Strain. 55,000X

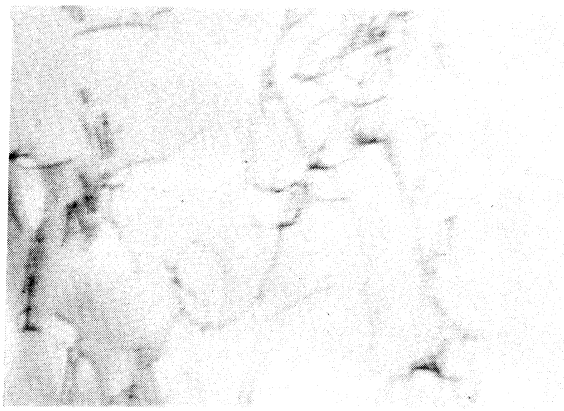

Figure 16. Regular and Irregular Networks Produced by Five Percent Unidirectional Tensile Strain. 55,000X

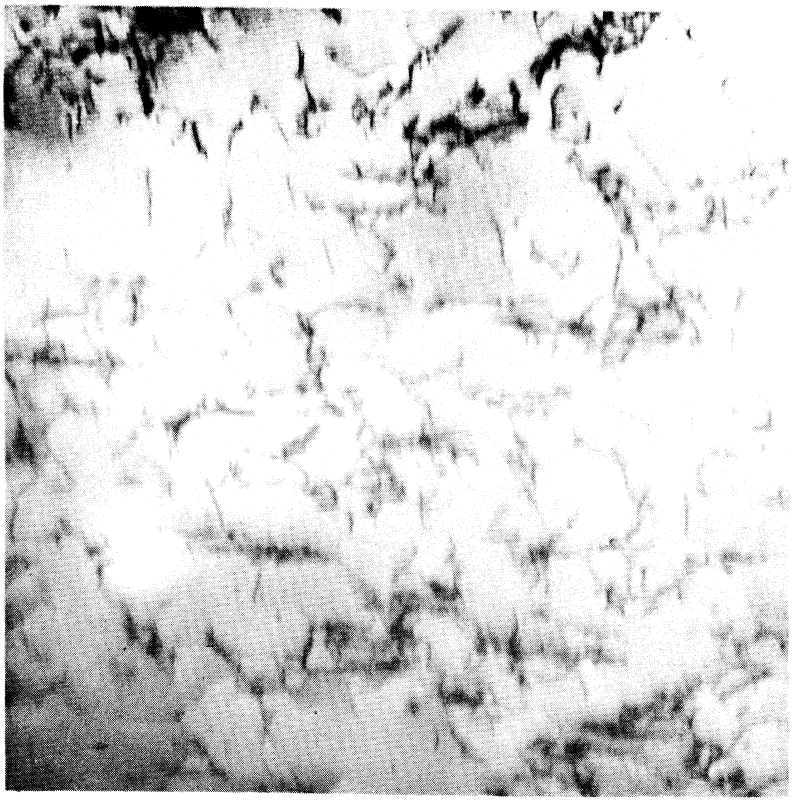

Figure 17. Typical Dislocation Arrangement Produced by Five Percent Unidirectional Tensile Strain. 35,000X

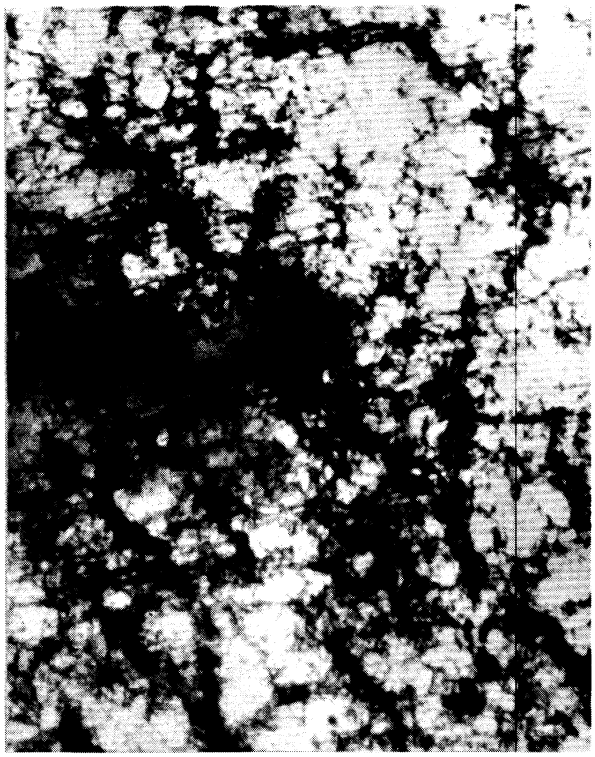

Figure 18. Cellular Structure of Dislocation Tangles Formed by 10 Percent Unidirectional Tensile Strain. 25,000X

Figure 19. Cellular Structure of Dislocation Tangles Formed by 20 Percent Unidirectional Strain. 25,000X

Figure 20. Stacking Faults and Dislocation Tangles Formed by 20 Percent Unidirectional Tensile Strain. 17,000X

Figure 21. Typical Region in the Tensile Fracture Specimen. 20,000X

to form both regular and irregular networks. It appears that the effect of these interactions was to greatly increase the stress as is evidenced by the relatively steep slope of the stress-strain curve at strains of 0.5 to five per cent. With the decreasing slope of the curve, cell structure of dense dislocation tangles as well as regions of numerous stacking faults appeared. At fracture small cell structure similar to that found at lower strains was not observed; instead, larger cells with extremely dense and thick walls of dislocation tangles as seen in Figure 16 were found. Apparently, the effect of increased strain in pure tension was to sweep the smaller cells into single large cellular arrangements of dislocation tangles.

4. Results from Specimens Deformed by Fatigue Loading

Basic differences were observed in the dislocation distributions present in specimens which were fatigued at different strain levels.

a. Low Strain

At low strain the specimen was fatigued at 1050 micro-inch/inch strain and 5.5×10^6 cycles. The thin foils obtained from this specimen contained dislocation pile-ups and a relatively low density of dislocations. Electron transmission micrographs of these foils are shown in Figures 22 and 23. Figure 22 is interesting in that it shows the projections of slip steps at an internal grain boundary. It is difficult to determine whether these lines result from slip steps in both grains or if they are in only one of the grains. The same type of phenomenon was reported by Hirsch, Partridge and Segall[33] for surface slip in fatigue at low stress levels and for surface slip in unidirectional tension. The important difference here is that the surface in this case is an internal grain boundary. It

is thus possible that the steps are associated with void regions at the grain boundary and that these voids are essentially intercrystalline cracks. The formation of these slip lines was probably due to the passage of a number of dislocations, and the vacancy atmospheres associated with them into the region of the grain boundary. This could possibly provide a means of internal crack initiation for failure at very low strain fatigue in the same manner as for surface crack initiation. This also supports the view that the initiation of failure does not necessarily occur at the specimen surface. The slip steps could have been made possible through the type of damage which the specimen received at the low strain level. The damage was not very severe and dislocations were either arranged in pile-ups or were rather well defined within slip systems. If dislocations that are arranged in either of these two fashions become pinned at the grain boundary surface, it is possible that they would rotate about the pinning point as a result of fatigue cycling and pass out through the grain boundary surface. Figure 23 is a micrograph of a region from another foil taken from the low strain fatigue specimen. This region is one of the more severely damaged regions that were observed in the foils from this fatigue specimen. Dislocation tangles and loops have formed and are readily seen in the micrograph. Although the tangles and loops are present, they still appear to be defined within certain slip planes as is evidenced by the well defined parallel lines of dislocations and dislocation tangles. At 5.5×10^6 cycles no banding or striation effect was observed. However, Hirsch et al.[33] found striations in stainless steel at 10^7 cycles for low stress levels.

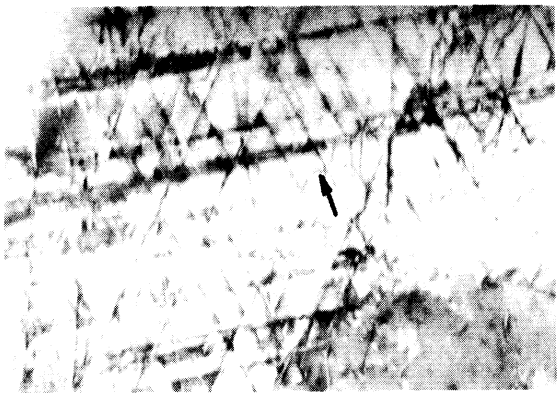

Figure 22. Slip Steps at an Internal Grain Boundary of a Low Strain Fatigue Specimen. 12,000X

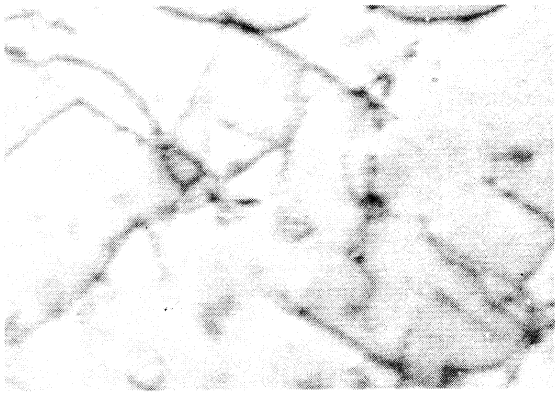

Figure 23. Transmission Micrograph of a Region of Relatively High Damage Formed at Low Strain and 5.5 x 10^6 Cycles. 24,000X

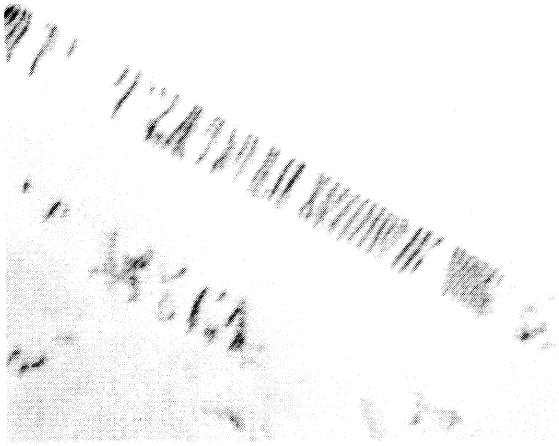

Figure 24. Isolated Groups of Dislocation Pile-ups Formed During Fatigue at Medium Strain. 40,000X

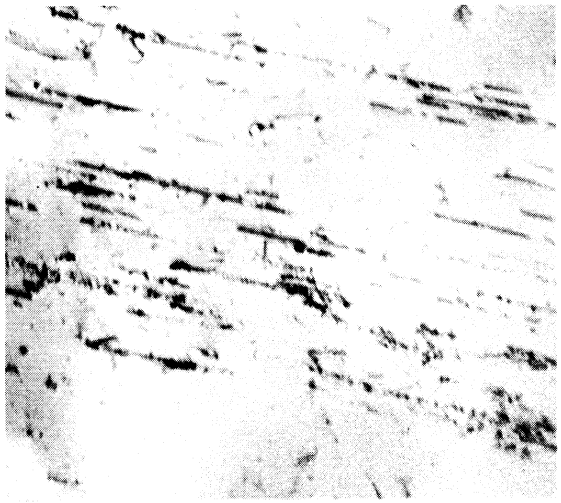

Figure 25. Segregated Bands of Dislocation Pile-ups and Stacking Faults Caused by Fatigue at Medium Strain and 100,000 Cycles. 9,000X

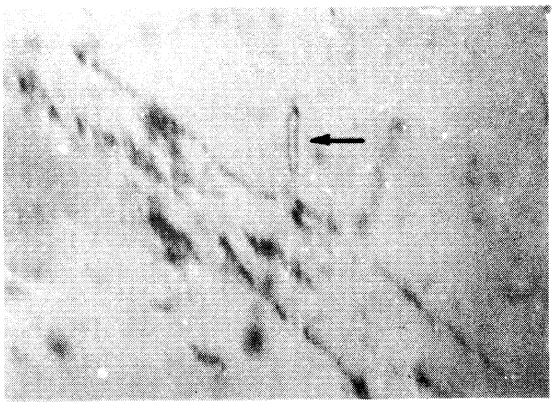

Figure 26. Dislocation Loop Observed in a Specimen Cycled for 100,000 Cycles at Medium Strain 15,000X

b. Medium Strain

At the 1600 micro-inch/inch strain level a very definite pattern of heavy banding was observed as is shown in Figures 25 to 30. The bands increased in density and width as the number of cycles was increased. Failure occurred at 10^6 cycles at this strain level. The first 5,000 cycles resulted primarily in dislocation pile-ups similar to those shown in Figure 24. There were many regions in the foils in which the density of dislocations was very low and the material had the same appearance as the annealed foils. The pile-ups shown in Figure 24 appear to be forming into compact groups within the planes of the pile-ups. These pile-ups are relatively far away from the grain boundary and do not extend to the grain boundary. These factors could possibly have significance in that such pile-ups would not be expected to result from long range movement of dislocations. A possible implication of these observations is that the pile-ups may have formed as a result of relatively small to-and-fro motion of individual dislocations. This would seem reasonable in view of the small plastic deformation that occurs during the fatigue cycle and the dependence of the density of these pile-ups upon the number of cycles as reported below. At 100,000 cycles the foils showed bands of dislocation pile-ups and stacking faults which are seen in the low magnification micrograph of Figure 25. The dark bands are regions of stacking faults and dislocation pile-ups which lie in the $\{111\}$ planes. The normal to the surface is in the $\langle 110 \rangle$ direction. Figure 26 shows a distinct example of a dislocation loop which may have resulted from the generation or migration of vacancies to form a vacancy cluster which collapsed into the loop, or from the interaction of a

dislocation with a point defect.[17] Dislocation loops were very apparent in the medium strain specimens which were fatigued at or above 100,000 cycles. The damage observed at 100,000 cycles was not predominantly dislocation tangles but instead was primarily segregated bands of stacking faults and dislocation pile-ups. Therefore, it is probable that the machanisms of interactions with point defects such as vacancy clusters to form dislocation loops were not the only cause of these loops, but that the mechanism of a vacancy disc collapsing to form a loop was also significant at medium and low strain. Examples of apparent dislocation interactions with point defects have, however, been observed and are shown in Figure 31.

An increase in number of cycles to 550,000, resulted in denser bands which were more closely spaced than at a lower number of cycles. Micrographs of typical damage conditions experienced at 550,000 cycles are shown in Figures 27 and 28. The bands contain numerous stacking faults, dislocation pile-ups, and regions of dislocation tangles and prismatic dislocation loops. The bands are very close together and appear to be linked by relatively long dislocations and isolated stacking faults. This trend of formation persists with further cycling as is shown by the micrographs of foils taken from a region near the crack of the failure specimen (Figures 29 and 30). Only one instance of tangles forming a cellular structure was observed at the medium strain level. Most of the tangles were within the dense regions of dislocation pile-ups and stacking faults which formed the bands. This band structure of tangles, faults and pile-ups appeared to be characteristic of the material fatigued at this

Figure 27. Bands of Dislocation Tangles and Stacking Faults Formed at Medium Strain and 550,000 Cycles. 20,000X

Figure 28. Interconnected Bands of Dislocation Tangles, Pile-ups and Stacking Faults Resulting from Medium Strain and 550,000 Cycles. 20,000X

Figure 29. Defect Present in the Specimen Failed at Medium Strain. 15,000X

Figure 30. Typical Bands of Extremely Dense Defect Structure in the Specimen That Was Failed at Medium Strain. 15,000X

strain level. It should be pointed out that this strain level just exceeds the proportional limit of the material and at this level of strain, pile-ups are virtually the only damage experienced at 1/4 cycle.

c. High Strain

The fatigue tests at high strain were run at strain levels of 3,000 micro-inch/inch and 5650 micro-inch/inch giving fatigue lives of 85,000 and 11,000 cycles, respectively. The most striking feature observed in the foils obtained from these specimens was the formation of a cellular structure of dislocation tangles as shown in Figure 35. Here again the formation of dislocation tangle structure was dependent upon the number of cycles of reversed strain. At the 3,000 micro-inch/inch strain level formation of the cellular structure was first observed at 5,000 cycles. Certain features in the buildup of this cell structure of tangles were observed with respect to the <110> normal. Micrographs showing the sequence of cell formation by dislocation tangles are shown in Figures 31 through 34. In Figure 31 the apparent interaction of dislocations with point defects and rotation of the dislocations in their plane to lie in the $\langle 10\bar{1} \rangle$ direction can be seen. The direction of this line is at an angle of 60° to the plane of the foil. This type of buildup was observed in the form of long straight lines of dislocations and dislocation tangles at 5,000 cycles and 3,000 micro-inch/inch strain. Figure 32 shows more developed lines of tangles connected to a grain boundary. Here the long dislocations tend to loop out of the $\langle 10\bar{1} \rangle$ direction into their slip plane. A still further developed condition is shown in Figure 33. The lines of dislocation tangles are more pronounced and dense dislocation tangles are beginning to appear. At this stage of

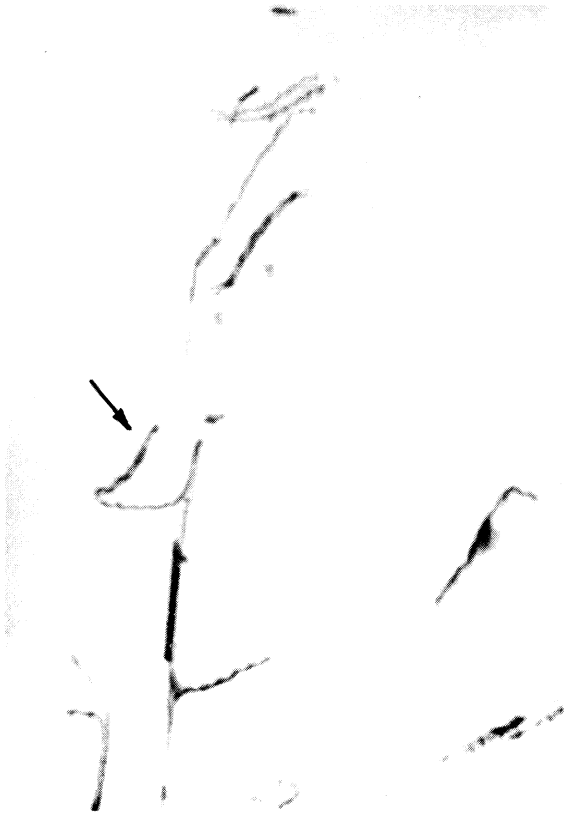

Figure 31. Beginning Formation of a Line of Dislocation Tangles During Fatigue. The normal to the foil is the <110>. 60,000X

Figure 32. More Developed Line of Dislocation Tangles. The foil normal is the <110>. 30,000X

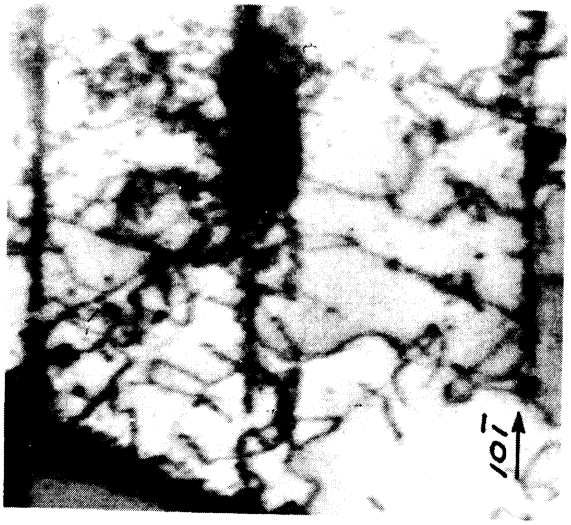

Figure 33. Formation of Dense Tangles of Dislocations and Dislocation Loops. 50,000X

Figure 34. Formation of a Cellular Structure of Dislocation Tangles. 30,000X

development heavier dislocation tangles are found in definite projected directions. These heavy tangles eventually become the cellular structure of dislocation tangles which were found to be predominant in high strain fatigue at higher numbers of cycles. Figure 34 shows the formation of a cell by these heavy tangles. The projected directions of the cell walls were deduced from the diffraction pattern of the micrograph and are indicated on the figure by an arrow. The cell structure that results from further cycling is shown in Figure 35. At a magnification of 200,000 X, dislocation loops and dislocation tangles are clearly resolved. The cell structure consists of dense walls of dislocation tangles and loops enclosing regions almost completely devoid of resolvable imperfections. Figure 36 is a high magnification micrograph of the failure condition at medium strain for comparison.

The results obtained at 3,000 micro-inch/inch strain prompted further work at higher strain. Accordingly, a series of fatigue tests at a strain of 5650 micro-inch/inch was undertaken in hopes that the initiation and formation of the cellular structure might be defined to lie within a given number of cycles. The fatigue tests were run at 11,000 (fracture), 1000, 200, 50 and 10 cycles. Typical areas for these conditions are shown in Figures 37 through 42. The first appearance of well developed cellular tangle structure was observed in the specimens fatigued at 200 cycles. Therefore, these cells have apparently formed between 50 and 200 cycles of reversed strain. A high density of dislocations was observed in the specimens fatigued at 10 cycles as shown in Figures 37 and 38. At this number of cycles the dislocations form a distinct array within the acting slip planes. An increase in the number of cycles to 50

Figure 35. Cellular Structure of Dislocation Tangles Formed at High Strain. Numerous dislocation loops and individual tangles can be seen. 200,000X

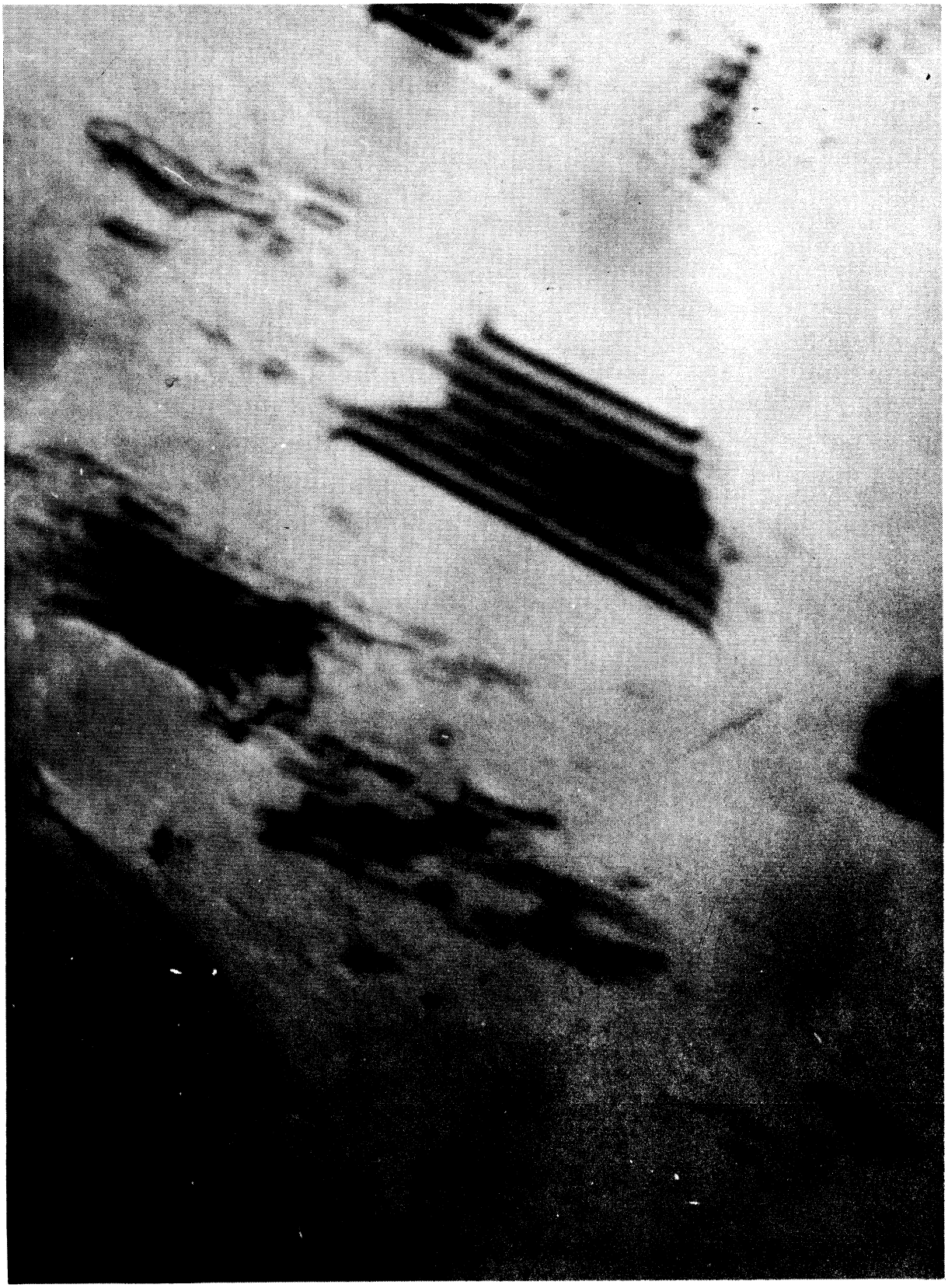

Figure 36. Stacking Faults Resulting from Fatigue at Medium Strain and 10^6 Cycles. 180,000X

produced a tendency for knotting of dislocations and for the formation of linear arrangements of heavy knots and tangles of dislocations as shown in Figure 40. These tangles were regularly spaced and were present primarily in one direction with lines of dislocations and less dense dislocation tangles connecting them at less regular intervals.

Figure 41 and 42 show regions of damage obtained at 200 cycles of reversed strain. At this condition of fatigue a definite cellular structure was apparent in many of the grains. This cellular structure is regular in its arrangement and consists of walls of heavy tangles surrounding regions of low dislocation density. The arrangement of the dislocations in the internal portion of the cells at this cycle level consisted of loops and long lines of dislocations. In many cases the dislocation lines extended completely across the cell. The direction of this pattern was consistent throughout each grain. Further cycling at this strain level resulted in a coalesence of dislocations at the cell walls and a sweeping clean of most remaining long dislocations from within the cell as can be seen near A in Figure 45.

Another type of dislocation distribution was found to result from fatigue at high strains. In some instances it appeared that some of the cell walls tend to sweep clean and that the dislocations that formed these walls migrated to the other walls leaving an elongated cell structure. In some instances the total grains appeared as uniform lamellae of dense tangles and dislocation free areas. Their appearance was very similar to coarse pearlite when viewed through a light microscope. This pattern can be seen in some of the grains in Figure 43 and in Figure 44.

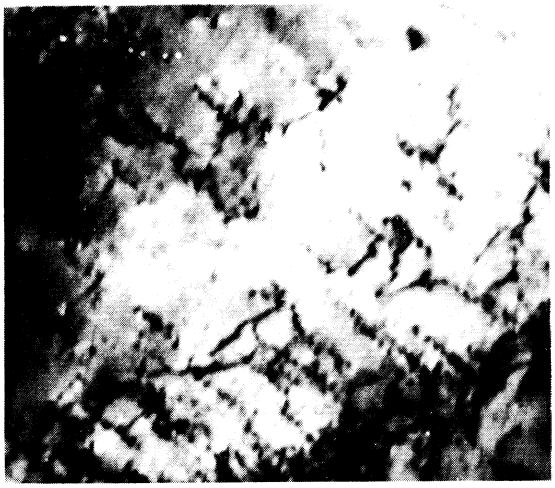

Figure 37. Typical Region Formed by 10 Cycles of Reversed Strain at 5650 Micro-Inch/Inch Strain. 25,000X

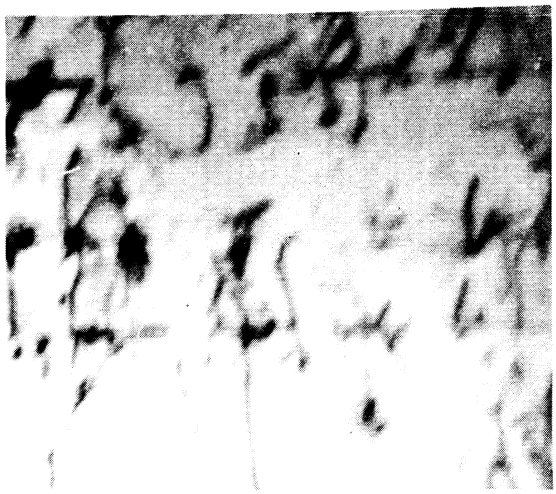

Figure 38. Micrograph of an Area Showing Interactions and Dislocation Tangles Formed by 10 Cycles at 5650 Micro-Inch/Inch Strain. 30,000X

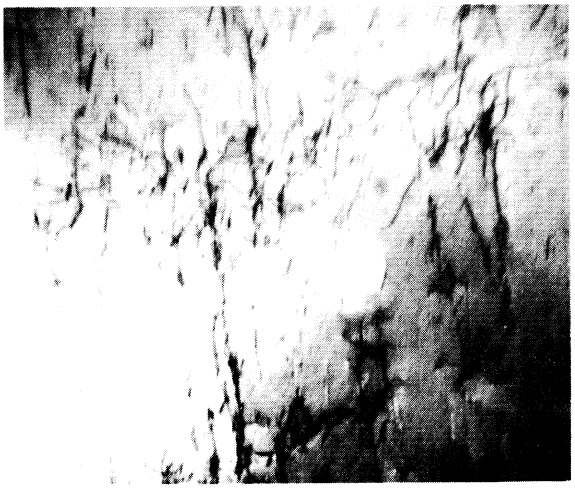

Figure 39. Condition of Damage at 50 Cycles of 5650 Micro-Inch/Inch Reversed Strain. 18,000X

Figure 40. Tangles Formed by 50 Cycles at 5650 Micro-Inch/Inch Strain. 18,000X

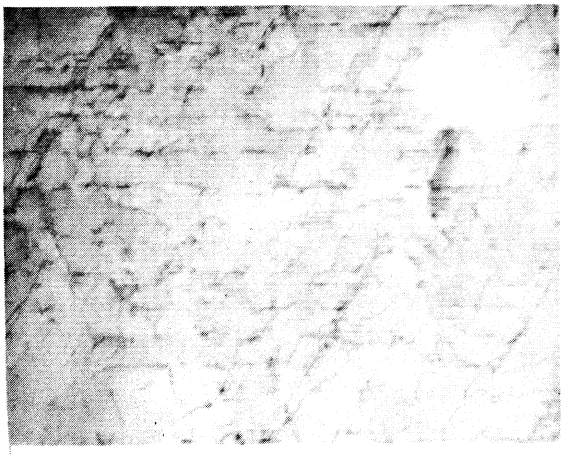

Figure 41. Regions of Dislocations and Tangles on Preferred Slip Planes at High Strain. 12,000X

Figure 42. Cell Structure of Dense Dislocation Tangles Resulting from 200 Cycles at 5650 Micro-Inch/Inch Strain. 21,000X

Extremely dense rows and cells of dislocation tangles were predominant in the specimen that was cycled for 11,000 cycles at 5650 micro-inch/inch strain. Fatigue at this level resulted in innumerable cracks not only at the surface but throughout the specimen. These cracks were both intercrystalline and transcrystalline. The size of these cracks was such that they were resolvable by the naked eye. During electropolishing of these specimens, polishing occurred preferentially in the region of the cracks and the metal was dissolved away from the cracks. Therefore the observations were probably made near but not at the regions of maximum damage.

An example of a typical area at low magnification is shown in Figure 43. This micrograph is taken from a thinned area several times larger than that represented by the micrograph. Most of the various types of arrangements of dense dislocation tangles which were observed in the foils are represented in this micrograph.

Another phenomenon which was observed in the specimens which failed at 3000 and 5650 micro-inch/inch strain was the formation of a definite structure of subgrains. Variation in contrast from subgrain to subgrain indicated that a definite boundary was present. Tilting of the specimen was also employed to verify that these were actually subgrains. Figures 45 and 46 show the subgrains. In Figure 45 it is apparent that these subgrains evolve from the heavy tangles. The region where the dense tangles are still present is shown at A. The region around B contains both cells of tangles and subgrains. The region of subgrains is shown at C.

Figure 43. Typical Distribution of Tangles and Damage Present in the Specimens Failed at 3000 and 5650 Micro-Inch/Inch Strain. 2,500X

Figure 44. Rows of Dense Tangles Resulting from High Strain Reversed Cycling. 30,000X

Figure 45. Micrograph Showing Cellular Structure of Tangles and Subgrains. The cellular tangles are at A and the subgrains are at C. 22,000X

Figure 46. Subgrains Found in the Failure Specimens Fatigued at High Strain. 10,000X

Grosskreutz and Waldow[26] have found subgrain formation to always occur ahead of the propagating crack in fatigued aluminum. They have concluded that subgrains will always exist at the tip of a fatigue crack in a high stacking fault energy material. It is also possible that subgrains are always present at the tip of the propagating crack in fatigued stainless steel. However, this conclusion cannot be made from the results of this study.

5. Studies Made of Foils Obtained from the Surface of the Fatigue Specimens

In order to study the dislocation distributions at the surface and compare them to the distributions below the surface, some of the specimens* were electropolished from one side only after fatigue cycling. The method used for electropolishing was exactly as outlined earlier except that one side was coated with "Microstop" lacquer during both the electropolishing steps.

The results obtained were inconclusive. Although the general patterns of dislocations were the same as below the surface, there appeared to be a definite loss or break up of the dislocation tangles at the surface. An illustration of this is given by the low magnification micrograph of Figure 48. In this micrograph (taken as representative of an area at least 10 times as large as that shown) light traces of the cell structure of dislocation tangles can be seen within the grains. The density of the dislocation in the cell walls appears to be much less than that found below the surface. In order to determine the orientation for optimum contrast the foil was tilted through $\pm$ 20° and rotated prior to taking this micrograph. The foil was obtained from a fatigue specimen that was cycled for 200 cycles

*See Table I

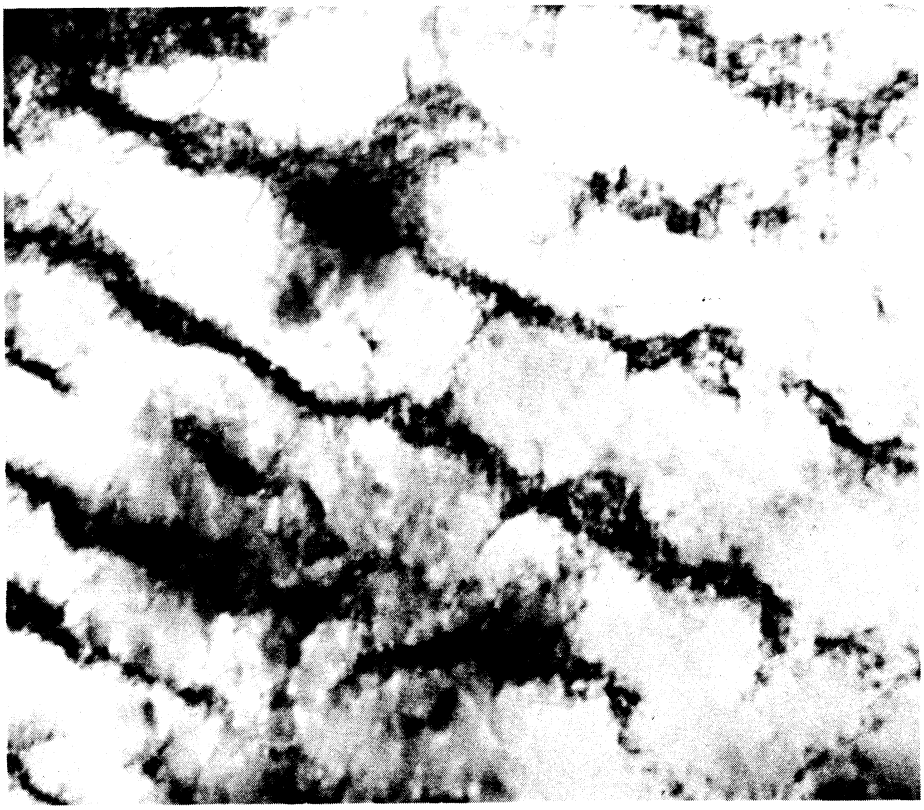

Figure 47. Transmission Micrograph Taken from Near the Surface of a Specimen Fatigued for 200 Cycles at 5650 Micro-Inch/Inch Strain. 40,000X

Figure 48. Low Magnification Transmission Electron Micrograph of a Foil Taken from the Surface of a Specimen Fatigued for 200 Cycles at 5650 Micro-Inch/Inch Strain. 3,000X

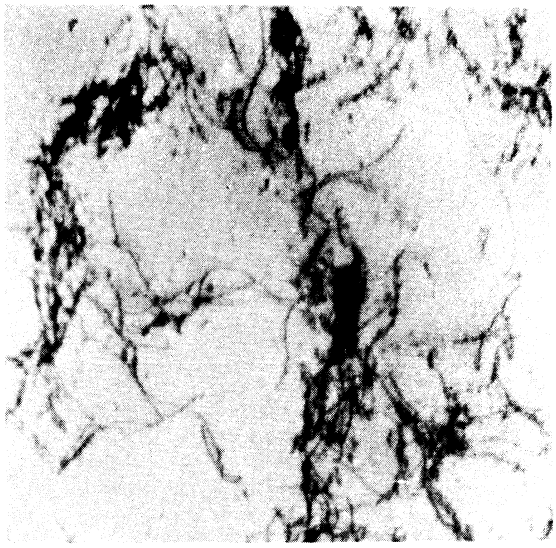

Figure 49. Transmission Electron Micrograph of a Foil Taken from the Surface of a Specimen Fatigued 1000 Cycles at 5650 Micro-Inch/Inch Strain. 30,000X

at the 5650 micro-inch/inch strain level. A comparison between the dislocation distribution at the surface and the dislocation distribution 0.001 inch below the surface can be made by comparing the density of dislocation tangles in Figure 42 with this micrograph. In the foils obtained from the surface of the fatigue specimens many grains were totally void of dislocations.

Figure 47 is another transmission micrograph taken at the surface of a specimen that has been cycled for 200 cycles at a strain of 5650 micro-inch/inch. Figure 47 shows rows of dislocation tangles and a tendency for the tangles to be less dense near the surface than below the surface. In some regions they appear to have been lost completely. Comparison of this micrograph with Figures 42 and 44 suggests that there has been a considerable amount of loss of dislocations near the surface.

Figure 49 shows a cellular tangle produced at 1000 cycles and at a strain level of 5650 micro-inch/inch. Here too, is found evidence of a break down of the tangles, or possibly an incomplete build up of a cell at the surface. For this condition of fatigue the cellular structure is usually very complete at 0.001 inch below the surface. A typical region at 0.001 inch below the surface corresponds to the subcells in Figure 35. A condition of this nature can be expected to occur since the surface of the fatigue specimen should be much the same as a thin foil and allow vacancies to diffuse out of the surface by pipe diffusion. However, a difficulty arises in that not all grains of a foil thinned in this manner show such a definite dislocation loss. The reason for this difference can in part be attributed to the thin foil preparation technique. It is very probable that for some areas the masking material used did not adhere sufficiently to the

surface. Therefore, when a hole dissolved through the thin foil electro-polishing could have taken place on both sides of the foil, and thus polished the surface of the specimen in some areas.

The possibility that dislocation rearrangement after fatigue loading was greater in these foils than the foils taken 0.001 inch below the surface is not likely to exist since the handling was essentially the same and particular care was taken to assure that the micrographs and observations were obtained from thicker regions of the foils.

DISCUSSION OF OBSERVATIONS

1. Relation of Fatigue Damage to Tensile Damage

Comparison of the defect distribution resulting from fatigue to that resulting from pure tension is of considerable interest since pure tension is basically 1/4 cycle fatigue.

The types of damage which result under unidirectional tensile strains may lead to a better understanding of the process of fatigue. From the results that have been obtained it appears that for 304 stainless steel three strain conditions of fatigue should be used for comparison of damage from fatigue to that resulting from unidirectional tension. These three strain conditions are 1) low strain which gives fatigue lives greater than 10^7 cycles, 2) moderate strains slightly above the proportional limit which correspond to lives of the order of 10^6 cycles, and 3) high strains which correspond to fatigue lives of 10^5 cycles or less. Hereafter, in this discussion, these conditions of strain will be referred to as Class I, Class II, and Class III fatigue respectively.

The results obtained for the Class I fatigue condition are incomplete in that the failure condition was not attained at the strain of 1050 micro-inch/inch. However, comparisons of damage can be made for the number of cycles that were obtained. The strain of 1050 microinch/inch is substantially below the yield strain of the material. At this strain the dislocation arrangement for pure tension should be much the same as that of the annealed unstressed material. Cycling at 5.5×10^6 cycles resulted in a damage condition similar to that obtained

at less than one per cent strain in unidirectional tension. The similarity of these conditions of pure tension and Class I fatigue can be seen by comparing the dislocation arrangements shown in Figure 38 and 13. At this level of tensile strain, interactions by dislocations from different slip planes are apparent and network formation begins. The tendency for band formation was not observed in the foils of the fatigue specimens. This result is rather interesting in light of the results obtained for Class II fatigue.

In Class II fatigue, the damage condition is characterized by the formation of bands of dislocation pile-ups and stacking faults. These bands appeared at a low number of cycles and increased in density and width, with further cycling. Dislocation tangles were observed to be more predominant in the specimens cycled at 550,000 and 10^6 than at 100,000 cycles. Pure tension at this level of strain resulted in the formation of dislocation pile-ups at the grain boundaries, and little or no interaction between dislocations or dislocation pile-ups that were present on different slip systems. It appears then, from a comparison of tensile damage just above the proportional limit to the damage produced by fatigue loading at various numbers of cycles for the same strain level, that the mode of damage was basically established in the first 1/4 cycle by the manner in which the dislocations pile-up at that time. It might be expected that the movement of the dislocations that were present during plastic deformation in the first 1/4 cycle of strain would establish paths of dislocation trails in the operating slip systems. These could then provide a source of dislocations during further cycling.

The dislocations distributions found in pure tension at strains corresponding to the strain levels of Class III fatigue consisted of pile-ups of dislocations lying in several different slip systems, and interactions of individual dislocations from various slip systems. Results of fatigue loading at this strain level differed considerably from that of Class II in that a cellular structure of dislocation tangles was formed. The formation of this cellular structure is probably related to the activation of slip on more than one slip system. The slip systems that are activated in the first 1/4 cycle of fatigue could basically serve as sites for the formation of the cell walls.

It is entirely reasonable that the first 1/4 cycle establishes the long range type of damage in a metal that is subjected to fatigue deformation. This appears to be the only similarity between the dislocation arrangements found in Class II or Class III fatigue and pure tension.

The dissimilar arrangement of dislocations in pure tension and fatigue has been reported by others for various metals[48,49] and by Hirsch, Segall and Partridge[33] for initially thin (0.005 - 0.012 inch) 18/8 stainless steel. In view of the results obtained in this investigation and those previously reported it appears that there is no relationship between the variation in dislocation distributions resulting from cummulative strain in fatigue to the dislocation distributions produced by unidirectional tension at high strain.

2. Comparison of Damage Produced at Various Strains and Cycles

The type of dislocation arrangements that result in 304 stainless steel during fatigue is dependent upon the level of strain and the number of cycles of strain. A comparison of damage at different strain levels can be made from the micrographs of Figures 30 and 43. The medium strain level of 1600 micro-inch/inch resulted in a band structure which increased in width and density of imperfections with increasing cycles up to failure. The fatigue strains of 3000 and 5600 micro-inch/inch resulted in a cell structure very closely related to that reported for pure metals.[24,25,26,48] Results obtained at strain levels of 1050 micro-inches/inch are not used for comparison here since the failure condition was not attained at this strain level.

Conclusions about the actual mechanism of failure initiation cannot be deduced from the results of this investigation. However, in as much as the types of dislocation arrangements differ considerably, the results may possibly be used to predict a variation in the method of fracture propagation at the two levels. In Class III fatigue the condition was one of a bulk weakening of the material. The failure appeared as almost a total collapse of the specimen in the region of the failure crack, with cracks initiating from a seemingly infinite number of points. The number of cycles that elapsed from the time of the first visual evidence of the failure crack until total failure was less than 10 at 5650 micro-inch/inch and less than 50 at 3000 micro-inch/inch. The fracture was observed to be transgranular as well as intergranular. It can reasonably be expected that the transgranular failure follows the tangle walls.

The condition in Class II strain could possibly result in transcrystalline failure propagation along the bands. The crack propagation would require an intercrystalline portion to allow for the variation in orientations of the grains.

In Class III fatigue, the dislocation arrangements which eventually formed at a given strain were well developed at a low percentage of the specimen life. At the 5650 micro-inch/inch strain level the cellular structure was present at less than one per cent of the fatigue life while at 3000 micro-inch/inch strain the cellular structure was present at approximately six per cent of the fatigue life. The size of this cellular structure did not appear to vary greatly with strain amplitude or number of cycles. The walls of the cells, however, became more "packed" as the number of cycles of strain was increased.

A comparison of the foils from the fatigue specimens which failed at high strains showed the structure for 3000 micro-inch/inch strain at failure to be essentially the same as the structure at 5650 micro-inch/inch strain at failure. Therefore, it was concluded that the structure is independent of the number of cycles in Class III fatigue.

The formation of heavy dislocation tangles lying in parallel rows as shown in Figure 40 might at first seem to be a totally different arrangement than that of the cellular structure. If this were the case it could be hypothesized that these lines are the images of dense tangles surrounding persistant slip bands in the fatigued metal. However, another possible explanation for this pattern can be found by considering the fact that the electron microscope in its present state of development cannot penetrate through metals which are much thicker than 3000-4000 $\mathring{A}$. Since

the cell size is on the average 0.6 - 1.0 micron or 6000 - 10,000 Å, a section 2000 Å thick through a cell wall could result in this type of image if the cells were lenticular instead of equi-axed. Since this same dislocation distribution was observed even at low cycle levels, (i.e. N = 200 for a strain of 5650 micro-inch/inch), the possibility that it results only from a migration of walls of tangles into the adjacent walls giving the heavy rows of dislocation tangles is not the answer.

3. Dislocation Uncertainty, Dislocation Tangles, and Mushrooming

Probably the most important recent advance in the theory of dislocations has been the dislocation uncertainty principle. It has been shown that for a dislocation an uncertainty of location exists which is normal to the dislocation axis, and is also in the slip plane of the dislocation.[69,71] This uncertainty results from the thermal vibrations of the atoms. In order words, dislocations can only be defined within regions instead of as lines. The magnitude of the uncertainty has only been defined[69] within the slip plane of the dislocations. However, an uncertainty must exist normal to the glide plane. Whereas an area of uncertainty must be present for all dislocations, the area of uncertainty will vary with the type of dislocation.

As a consequence of the uncertainty principle, the slip plane of the dislocation must possess an area of uncertainty. Moving dislocations can be expected, statistically, to transfer shorter or longer segments, together with their own uncertainty, to the adjoining

slip planes.[75] In this manner jogs and point defects can be formed by a moving dislocation. This concept, therefore provides an acceptable reason for the spontaneous accumulation of jogs by moving dislocations, even at low temperatures and in nearly perfect crystals.

Early theories of strain hardening are based primarily on the concepts of dislocation pile-ups. Electron transmission examinations of thin foils strained while in the electron microscope as well as other techniques[74] appeared to verify the early theories. Later, however, examinations on specimens thinned from the bulk conditions showed a structure of an entirely different nature. Observations showed a distribution of "clusters" or "birdnests" of tangled dislocations.[36] The reason for the difference is that the observations made on deformed thin foils were only characteristic of the dislocation distributions in thin foils, and not at all representative of the bulk condition of the material. This difference is probably the result of pipe diffusion by vacancies along a dislocation and out through the surface of the thin foil, or from the actual passing of a dislocation through the surface during straining of the foil.

In the bulk condition a sequence called "mushrooming"[71] can be expected to occur. Mushrooming is a multiplication of the number of imperfections caused by interactions among themselves when a crystal is subjected to deformations. All metals possess a number of point defects such as vacancies, vacancy aggregates, and interstitials[47] which can hold up a dislocation if the dislocation core meets the aggregate. These point defects may result from equilibrium conditions, quenching, or moving jogs.

A number of events which result in mushrooming can be summarized quite readily.

(1) A vacancy disc can form when a moving dislocation intersects a sufficient number of vacancy aggregates. The vacancy aggregates will add to the present vacancy atmosphere in the dislocation core and the stress field of the dislocation will aid the collapse of the vacancy aggregate to form a disc. These discs will appear as prismatic dislocation loops in a micrograph.

(2) The prismatic dislocation loops can either be formed to partly fuse with the original dislocation or be formed separate from them. If the loop is fused to the moving dislocation it will form a kink, and either pin the dislocation or move along with it. It is also possible that the fused loop can break completely free of the original dislocation and be left behind. If, however, the vacancy disc is formed separately from the dislocation core, the disc will remain behind in the form of a prismatic loop.

(3) Another method of prismatic loop formation which falls within the concept of mushrooming is the formation of loops by a moving dislocation when it meets a point defect.[17] The screw dislocations can form dislocation loops through the combined mechanisms of climb and glide.

The combination of these events causes birdsnests or tangles of dislocations to result.

4. Formation of Cellular Structure During Fatigue

The formation of the cellular structure of dislocation tangles during the fatigue process is an extremely interesting phenomenon.

Previously its occurrence in fatigued metals has been associated only with the metals which possess high stacking fault energies such as aluminum.[76,49,48] The presence of the cellular tangles in low stacking fault energy stainless steel fatigued at high strain may throw some light on the method of their formation during fatigue.

In order to better understand the particular conditions required for the formation of dislocation tangles in stainless steel, the known methods of jog formation which are necessary for point defect formation will be mentioned. In addition to jog and point defect formation through dislocation uncertainty, there are three other methods by which jogs can form. These three are climb, cross slip, and dislocation intersection. The movement of a jog formed in any of these manners will cause point defects in the form of vacancies or interstitials to result in the wake of the jog.[47]

The low stacking fault energy of stainless steel, however, can be expected to restrict the formation of jogs primarily to dislocation intersection and dislocation uncertainty mechanisms. The behavior of stainless steel, because of its low stacking fault energy, is such that cross slip and dislocation climb are not expected to occur on a large scale.[67] In fact, only one observation of the occurrance of cross slip in stainless steel has been reported.[13] Another characteristic feature of low stacking fault energy materials is a relatively low density of dislocation loops and point defects in the annealed condition.

The manner in which the cellular structure of dislocation tangles forms in this material is apparently through the process of mushrooming of dislocations once the initial point defects are formed. These point defects can be expected to form primarily through either dislocation interactions or dislocation uncertainty. The formation of jogs and point defects through climb and cross slip cannot be ruled out entirely since the strain level and temperature at which the cellular tangles were observed are relatively high. The importance of climb and cross slip to cellular tangle formation, however, could be determined through electron transmission examinations of specimens fatigued at low enough temperatures and cycle rates to assure that these mechanisms are not operating.

If dislocation intersection were the main cause of point defect formation, there should be a tendency for the dislocation tangles to occur more heavily at the intersections of the activated slip systems. This, however, does not seem to occur. The dense tangles which eventually form the subcell, as observed in Figure 33, appear almost independently in the activated slip planes. It also appears that these dense tangles are relatively independent of the dislocations that are not within the tangle. This too can be seen in Figure 33. Here the dislocation density in regions near the dense tangles does not vary greatly from the dislocation density near the regions of light tangles. This would seem to indicate that movement of jogs formed through dislocation intersection is not the basic method by which the point defects required for cellular tangles result. However, its significance would increase with an increase in the fatigue strain.

It seems therefore, that point defect formation through dislocation uncertainty plays a very important role in the formation of the cellular structure of dislocation tangles, and that its importance should increase with decreasing fatigue strains during Class III fatigue.

From the results it appears as if the mushrooming effects act mainly in the regions of the highly activated slip planes and that tangle formation and growth occur primarily in these regions. In other words the cellular walls are initially formed by a concentration of point defects through the movement of jogs. These regions of initial point defect concentration will mushroom and form the cell wall. The interior of the cells will always be a region of relatively low point defect density and random dislocation tangles may result there from interaction of the few dislocations that exist there with the point defects. Under such conditions, cellular structure can form with very small movements of dislocations. This would seem to be a necessary requirement of a model to explain cellular tangle formation during fatigue.

The ability of high stacking fault energy materials to cross slip readily at very low strains allows the formation of cellular tangles at strains corresponding to fatigue lives much longer than the lives at which cellular structure forms in stainless steel. In fatigue at medium strain in stainless steel only a few slip systems are activated and dislocations are confined to these slip systems because of the materials low stacking fault energy. These slip systems

are in the same orientation in each grain and cycling results in a banded structure which parallels these slip systems. Dislocation tangles, however, can result in these planes and mushrooming can still occur.

In view of the results obtained during this study, it is fairly safe to conclude that mushrooming plays a very important role in the formation of the dislocation arrangements which result in 304 stainless steel during Class II and Class III fatigues.

CONCLUSIONS

1. Cellular structures of dislocation tangles form in 304 stainless steel under the conditions of reversed bending fatigue at constant strain and fatigue lives less than 100,000 cycles.
2. Generation of dislocation loops is characteristic in fatigue at lives less than 10^6 cycles.
3. The average distribution of dislocation tangles is reduced near the surface of a specimen fatigued by reversed bending.
4. The dislocation distributions resulting from high unidirectional tensile strains are not similar to those which result in 304 stainless steel from fatigue loading for fatigue lives less than 10^6 cycles.
5. At high strains, the cellular structure of dislocation tangles formed during the early cycles of fatigue can transform into subgrains with further cycling.
6. At high strains the dislocation distributions at fracture are essentially the same independent of the fatigue life for 304 stainless steel.
7. The characteristic dislocation patterns that are formed early in the life of a fatigue specimen are developed more completely as the result of further fatigue cycling.
8. The dislocation distributions present in a failed specimen of 304 stainless steel that has been fatigued by reversed bending at medium or high constant strain are probably determined within the first few cycles.

SUGGESTED FUTURE WORK

The results obtained show that the initial cycles of fatigue greatly influence the dislocation distributions that result from fatigue. The degree to which the first few cycles influence the distrbutions of dislocations would be determinable by transmission studies of fatigued metal subjected to high strain for a certain number of cycles and then failed at lower strains.

Studies of the dislocation distributions that result during the phenomenon of coaxing in fatigue is another area toward which research should be directed. This may basically point out the dislocation distributions required for longer fatigue lives in materials. A distribution of dislocations which is relatively stable to fatigue deformation is present in coaxing. The determination of the type of distribution of dislocations which causes this effect would be a valuable step in understanding the basic mechanisms involved in fatigue. Since aluminum is a metal in which the phenomenon of coaxing occurs and since more is known about the dislocation distributions that are formed in this metal as a result of fatigue than in other metals, it would seem to be the most logical material to use for such a study. Loop patches predominate in this metal after fatigue at low strains, and subgrains result after fatigue at higher strains. It might be expected that the loop patches which result from the cycling at low strain during understressing would influence the volume and the shape of the subgrains that result from further cycling at the higher strain. The same type

of studies applied to overstressing might also help to understand the basic mechanisms involved in the fatigue process.

In addition to the above areas, work of the same nature as the work in this thesis should be continued. For example more data should be obtained, especially for fatigue at intermediate strains between Class II and Class III fatigue.

APPENDIX A

IMAGE FORMATION AND CONTRAST EFFECTS IN METALS

The formation of the image as observed in the electron microscope represents the electron intensity distributions at the bottom surface of the metallic foil. Since the intensity distributions and therefore the contrast in the transmission image is sensitive to atomic positions in the metal, displacements of the atoms in the regions of dislocations, stacking faults, and grain boundaries may be observed in the image.

Interpretation of the diffraction contrast that results when electrons are transmitted through a metallic foil is based on the dynamical theory and the kinematical theory of electron diffraction. The dynamical theory of diffraction considers the interactions which take place between the incident and diffracted electron beams and the atoms of the crystal lattice. The kinematical theory, on the other hand, gives an approximate theory of diffraction contrast of crystals which does not consider interactions of the diffracted beam with either the incident beam or the atoms of the crystal lattice. The kinematical solution becomes asymptotic to the dynamical solution of the theory of diffraction for (1) large enough deviations from the Bragg angle or for (2) very thin crystals. The dynamical theory has not yet been developed for crystals containing dislocations but it does present a solution for interpretation of contrast at stacking faults and thickness fringes in crystals. The kinematical theory, however, has been extended to provide a qualitative explanation of the contrast effects of imperfections observed in metal foils in the electron

microscope. For this reason a brief review of its fundamental aspects is presented here. More rigorous and more detailed explanations and derivations of this theory are found in the literature.[4],[32],[38],[55],[66]

1. The Reflecting Sphere

The conditions corresponding to reflection can be represented by a geometrical construction in the reciprocal lattice as shown in Figure 50. For this particular construction the incident beam and reflected beams are designated by $\bar{k}_o$ and $\bar{k}_1$ respectively, and the reciprocal lattice vector from the origin 0^* of the reciprocal lattice to the reciprocal lattice point r^* is $\bar{g}$. When a sphere of radius $1/\lambda$, where λ is the wavelength of the incident beam, touches the origin of the reciprocal lattice and intersects a reciprocal lattice point, the plane represented by this lattice point will be a reflecting plane provided the structure factor of this plane is not equal to zero. From Figure 50 it can be seen that

$$\bar{k}_1 - \bar{k}_o = \bar{g} .$$

In order that reinforcement of a reflected wave can result, it is necessary that the path difference of waves reflected by the same planes be an integral number times 2π. In the case shown in Figure 50 the path difference of two waves corresponds to the Bragg reflection and is given in vector form by

$$(\bar{k}_1 - \bar{k}_o) \cdot \bar{r}$$

where $\bar{r}$ is a vector in the direct lattice.

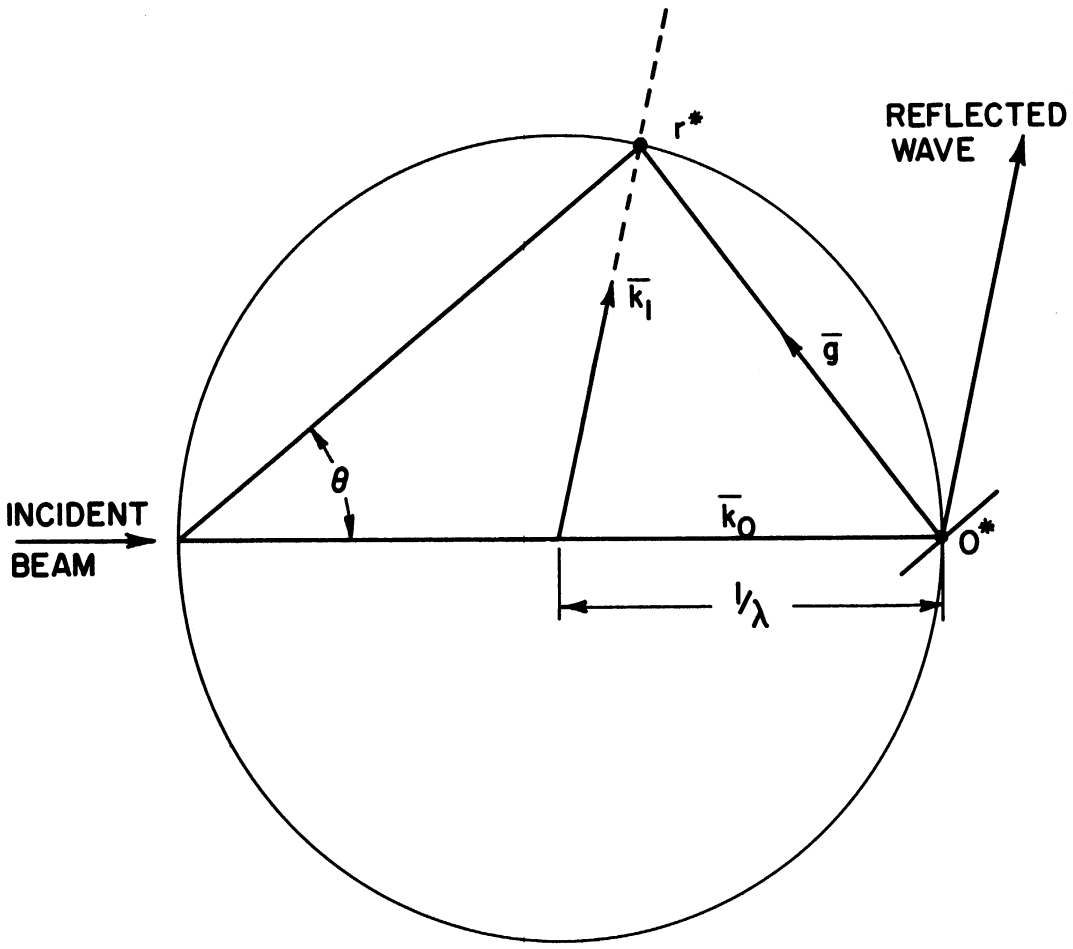

Figure 50. Sketch of the Reflecting Sphere for the Exact Bragg Condition of Reflection.

2. Phase Amplitude Diagrams

The uniform spacing of the atom positions in metals causes diffraction conditions which are similar to the diffraction phenomenon experienced by a diffraction grating. Consequently, the same methods can be employed for interpreting the contrast effects of electrons in metals as are used for interpretation of the illumination phenomenon in light rays. One qualitative method uses "vibration polygons" or "phase amplitude diagrams" to interpret contrast effects. Bendler,[4] following the work of Hirsch, Howie, and Whelan[32] has used this method to illustrate the electron transmission contrast effects in imperfect crystals. As the simplest example of the use of this type of diagram, the condition corresponding to reflection at the exact Bragg angle (Figure 50) is used. For this condition, assume as shown in Figure 52a that a wave of intensity I_o is incident parallel to the periodic row of reflecting units AD. The scattering that results depends upon the path difference of the wavelengths scattered by the successive atoms. In this example the waves are exactly in phase and vectors representing the diffracted waves are in line. The resultant amplitude is represented by $\overline{AD}$ in Figure 52a.

For the same condition of reflection the vector expression for the amplitude of the electron wave diffracted from one unit cell at the exact Bragg angle is given by

$$A = F_1 \exp(2\pi i \bar{g} \cdot \bar{r})$$

where F_1 is the scattering factor for one unit cell. This reduces to

$$A = F_1$$

because of the requirement that $\bar{g} \cdot \bar{r}$ must be an integer in a metal crystal. For a column of unit cells the amplitude is the summation over all the unit cells.

3. Deviation from the Exact Bragg Condition

The kinematic theory predicts the intensity of illumination for slight deviations from the Bragg angle. The sketch of Figure 51 shows this deviation with respect to the reflecting sphere. Vector addition gives the relation for small deviations as

$$\bar{k}_1 - \bar{k}_o = \bar{g} + \bar{s}$$

where $\bar{s}$ is a vector representing the deviation of the reciprocal lattice point from the reflecting sphere. The effect of this deviation is to cause a phase difference between the reflected waves from each successive reflecting unit cell. This particular condition can be shown by a vibration polygon. For successive reflecting unit cells, the total amplitude that results is a vector summation of the reflected waves from each unit cell. Figure 52b illustrates this summation for successive unit cells. Vectors $\overline{OA}$, $\overline{OB}$, $\overline{OC}$ and $\overline{OD}$ are termed closing vectors, and represent the total amplitude reflected by 1, 2, 3, and 4 unit cells respectively. The total phase difference between the waves is represented by the angle between the closing vector and the vector representing the first reflection.

If there is a sufficient number of reflecting units the vibration polygon will form a complete circle which will continue to repeat itself indefinitely. For each circle there will be a maximum amplitude

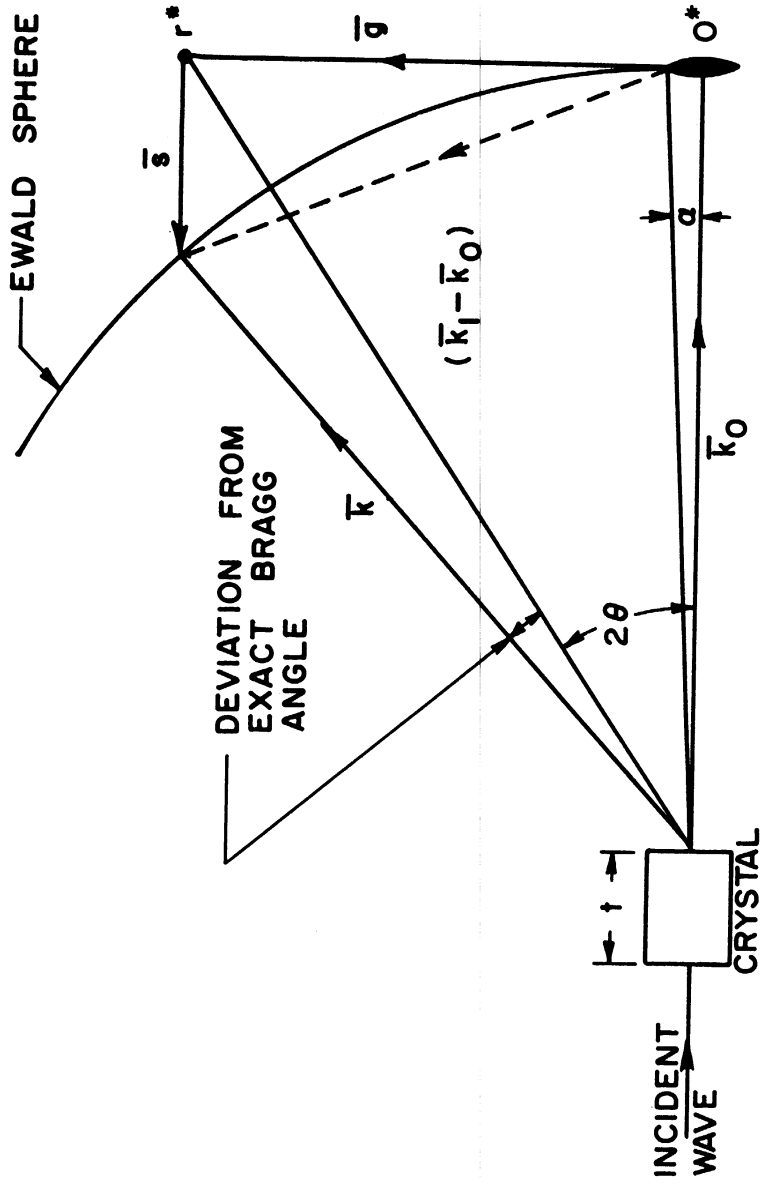

Figure 51. Deviation from the Bragg Condition at a Reciprocal Lattice Point.

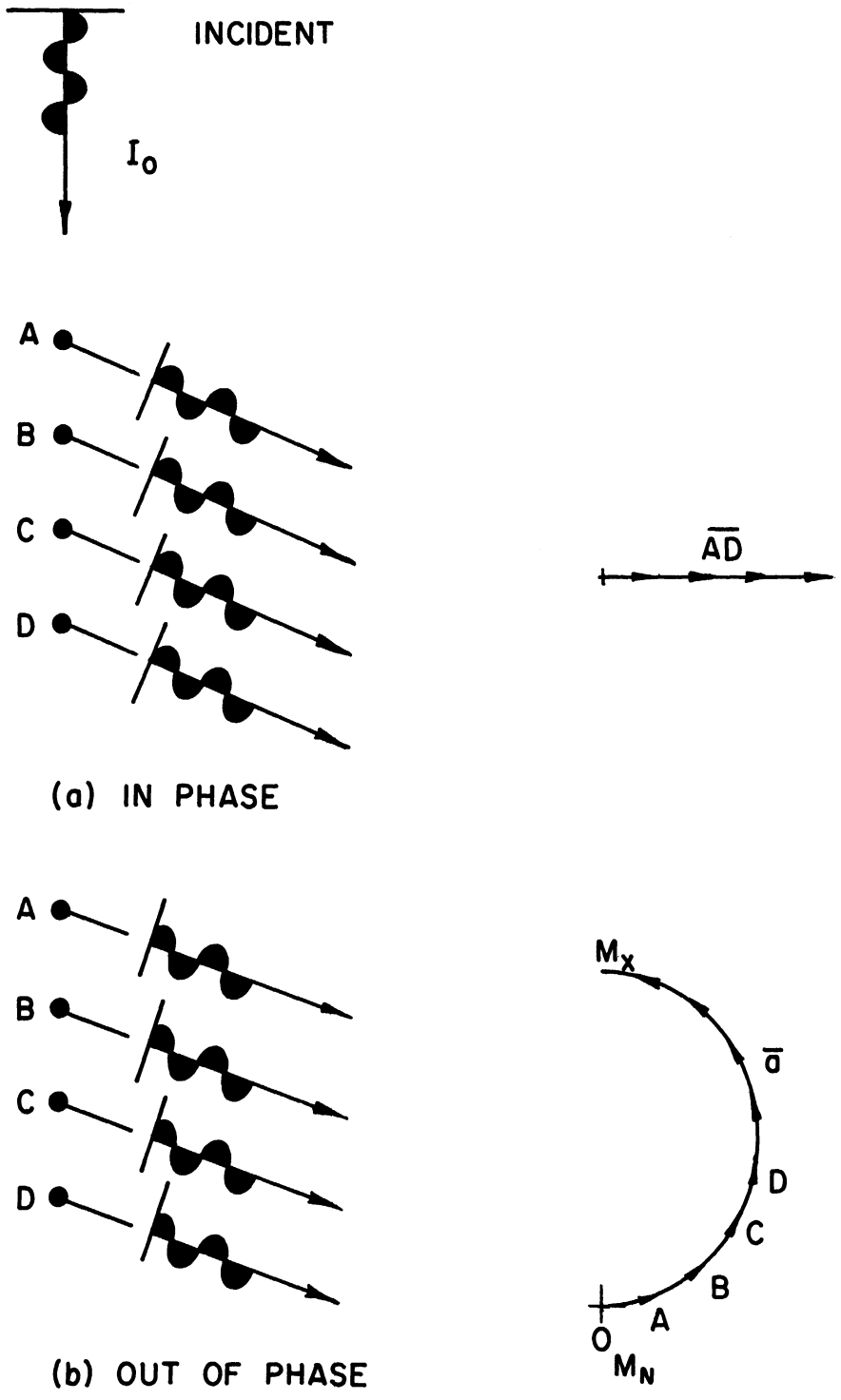

Figure 52. Sketch of Vector Polygons for the Two Reflecting Conditions of Figure 50 and Figure 51.

and a minimum amplitude which correspond to M_x and M_n on Figure 52b. These amplitudes exhibit a total phase difference $\sum \alpha_{max} = (n + 1/2)\,\pi$ and $\sum \alpha_{min} = n\pi$, where n is an integer. Therefore the maximum amplitude must occur when $\alpha = (n + 1/2)\pi$ and the minimum must occur when $\alpha = n\pi$. Since the angle α represents a constant phase difference, the resultant amplitude is given by

$$A = a \frac{\sin \frac{n\alpha}{2}}{\sin \frac{\alpha}{2}} \tag{A-1}$$

The intensity is given by the square of the amplitude or

$$I = a^2 \frac{\sin^2 \frac{n\alpha}{2}}{\sin^2 \frac{\alpha}{2}} \tag{A-2}$$

For this condition of reflection the mathematical vector expression for the amplitude of a column in a perfect crystal is

$$A = F \sum_n \exp(2\pi i(\bar{g} + \bar{s}) \cdot \bar{r}_n) \tag{A-3}$$

which reduces to

$$A = F \sum_n \exp(2\pi i \bar{s} \cdot \bar{r}_n) \tag{A-4}$$

because $\bar{g} \cdot \bar{r}_n$ is always an integer. Integration over the column length which corresponds to the thickness, t, of the foil gives

$$A \propto \frac{\sin \pi t s}{\pi s} \tag{A-5}$$

which is essentially the same expression as (A-1). The intensity, I, is proportional to the square of the amplitude. Therefore

$$I \propto \frac{\sin^2 \pi t s}{(\pi s)^2} \tag{A-6}$$

Equation (A-6) shows that the intensity is a periodic function of the thickness. It can also be seen from this equation that the illumination is periodic with respect to variation from the Bragg angle. The periodic dependence of the intensity on the film thickness, t, and the magnitude, s, of the vector $\bar{s}$ in Figure 51 has significance in interpretation of transmission micrographs. As a film thickness varies, dark and light line images result in the micrograph because of this dependence on thickness. These images are termed thickness extinction contours. However, if s varies while t remains constant, extinction contours will also be present. This latter condition corresponds to buckling of the foil.

4. Contrast Resulting from Crystal Imperfections

The reflecting sphere can be used to illustrate that the amplitude of the reflected waves from the unit cells near a simple edge dislocation is different than in the perfect crystal. Figure 53 shows the reflecting sphere for a column of unit cells near an edge dislocation. The subscripts (a) refer to the reflections of the unit cells in the portion of the column A which is not distorted, while the subscripts (b) refer to the reflections from unit cells in the distorted portion of the column near B which, in this illustration, satisfy the exact Bragg condition for reflection. In other words there are unit cells in the distorted column which are displaced such that their reflections compensate for the deviation from the Bragg condition of reflection which results in the undistorted column. Since the total amplitude depends on the reflections from all the unit cells in the column the image that results from a dislocation is a consequence of phase changes caused by the displacements of the unit cells in the region of the

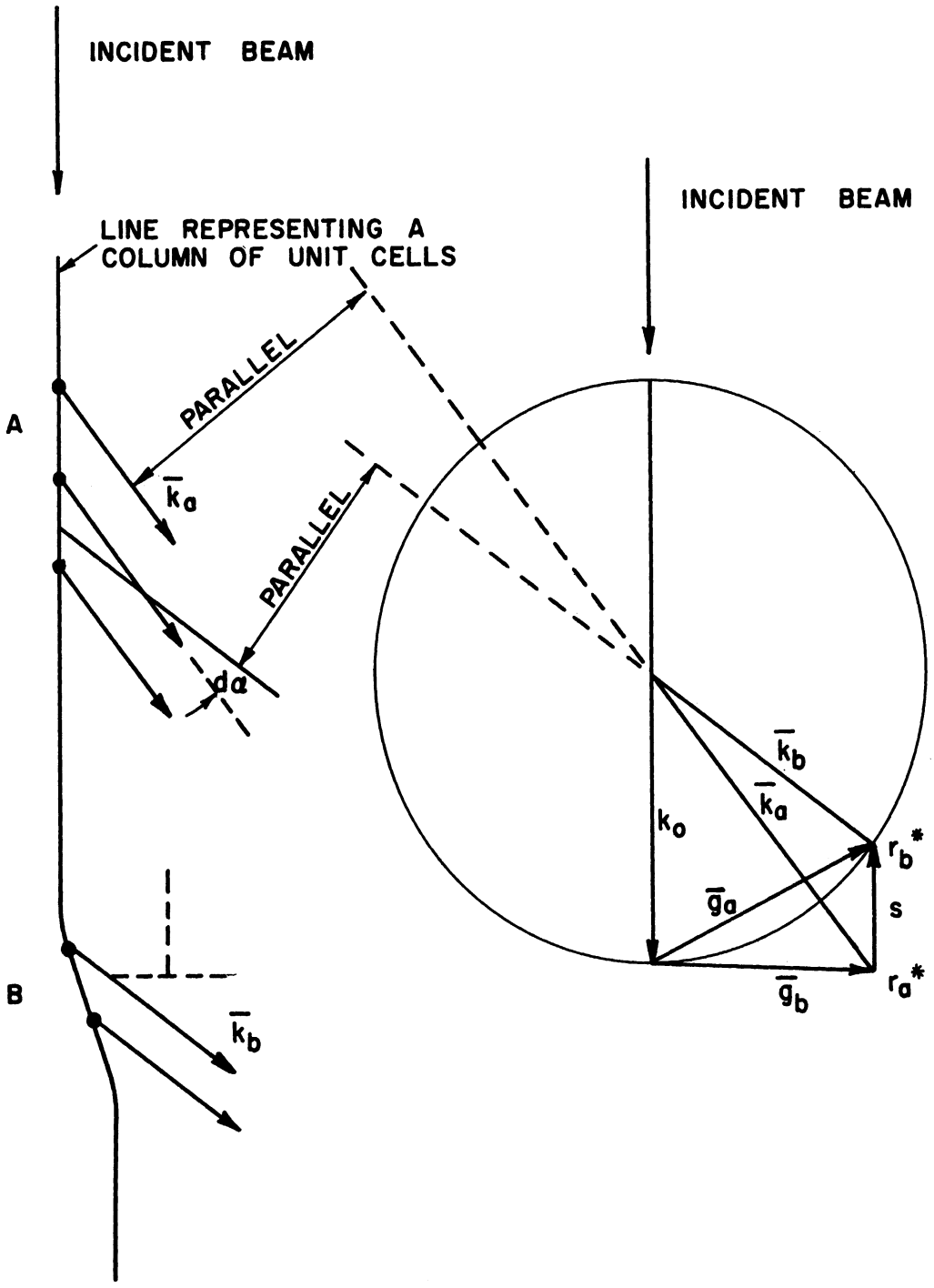

Figure 53. Sketch Showing the Origin of Contrast on One Side of an Edge Dislocation.

imperfections. This is illustrated by the vibration polygon of Figure 54. The base circle A corresponds to the reflecting unit cells in the portion of the column which is not affected by the imperfection. As the region of the imperfection is approached, the orientation of the unit cells will cause the vectors representing their reflection to depart from the circular path as a function of $\Delta\alpha$. When the region of distortion is passed, the vector polygon will again return to its circular periodic nature as represented by circle B . The phase angle shift in the vector polygon is a function of the displacement of the column in the region of the imperfection. The total amplitude for the column is given by the vector $\overline{OR}$.

An imperfection changes the vector expression for the amplitude of a column near the imperfection. If the displacement of the unit cells from their original reflecting condition is $\bar{R}$, the path difference of the successive reflections from the column is given by

$$(\bar{k}_1 - \bar{k}_o) \cdot (\bar{r}_n + \bar{R})$$

The expression for the total amplitude of the column becomes

$$A = F \sum_n \exp(2\pi i(\bar{g} + \bar{s}) \cdot (\bar{r}_n + \bar{R})) \qquad \text{(A-7)}$$

which reduces to

$$A = F \sum \exp(2\pi i g \cdot R) \quad \exp(2\pi i s \cdot r_n) \qquad \text{(A-8)}$$

when $\bar{s} \cdot \bar{R}$ is neglected (since these terms are very small compared to the other terms). Comparison of this equation with the equation for the perfect crystal (Equation (A-4)) shows that the only variation is $(2\pi i \bar{g} \cdot \bar{R})$

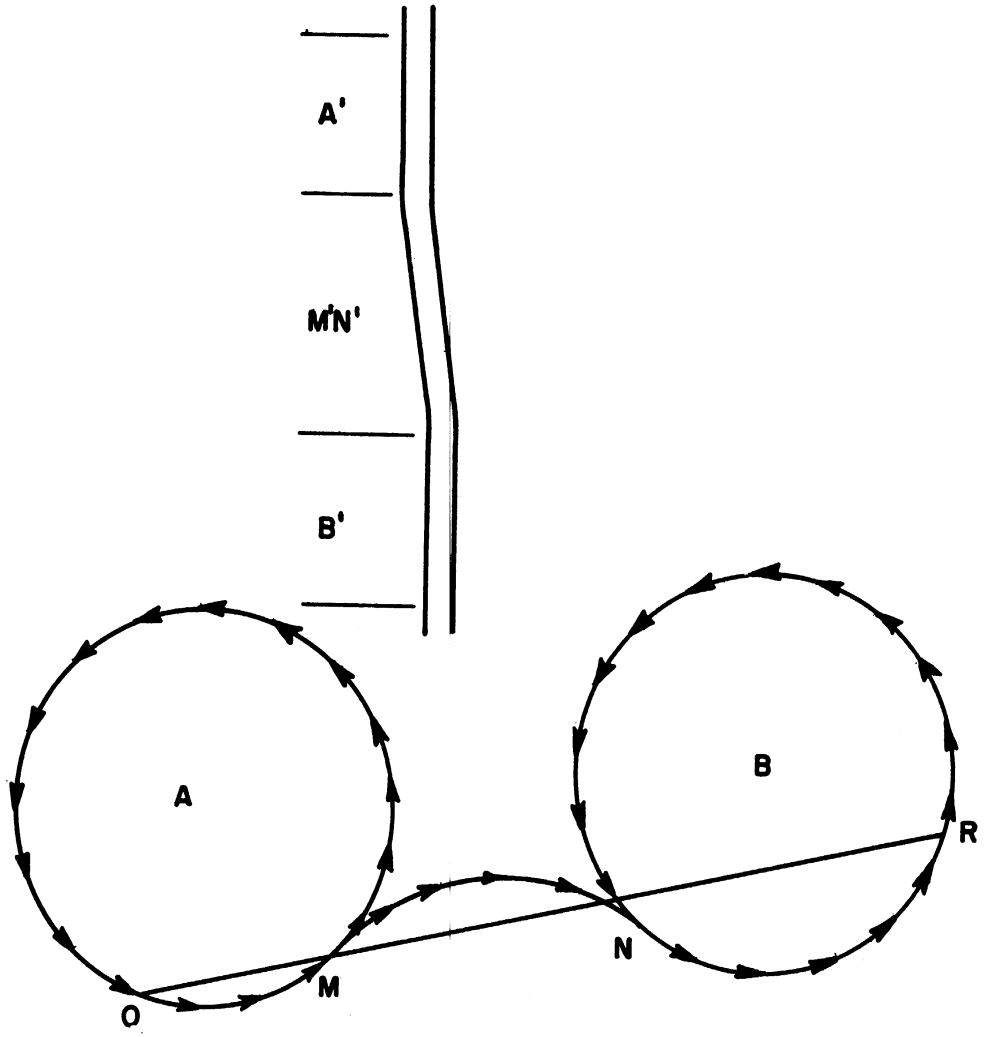

Figure 54. Sketch of a Vector Polygon Corresponding to the Amplitude of Reflection from a Column in a Region of Imperfection in a Crystal.

in the exponent. This is a phase angle variation α , which is a function of the location of the reflecting unit in a column.

Hirsch, Howie and Whelan[32] were the first to apply the kinematical theory to imperfections in crystals and their results are summarized below:

(1) The contrast from a mixed dislocation is similar to that from a screw dislocation.

(2) The image of an edge dislocation may be slightly wider than for a screw dislocation and dislocations should become narrower and less visible the more steeply inclined they are to the plane of the foil.

(3) The contrast peak is displaced to one side of the dislocation center by the order of magnitude of the dislocation width.

(4) When the burger's vector of a dislocation lies in the reflecting plane, the dislocation is invisible; i.e., when $\bar{g} \cdot \bar{b} = 0$, there is no diffraction contrast.

(5) The visibility of dislocations that are inclined to the foil surface may vary along its length giving a dotted pattern.

(6) For low order reflections the widths of the dislocations should be on the order of 100 to 200 $\mathring{A}$.

(7) Dislocations should appear dark in bright field and light in dark field microscopy.

APPENDIX B

INDEXING OF DIFFRACTION PATTERNS AND RELATION OF DIFFRACTION PATTERN TO MICROGRAPHS

In order to determine crystal orientations and directions in electron micrographs, use of electron diffraction patterns is necessary. The indexing of these patterns is systematic and their correspondence to the micrographs can be simplified by use of vector geometry. Accordingly, the fundamentals of the indexing procedure and necessary vector manipulations are outlined below.

1. In face-centered cubic crystals there are only a few types of permissible reflections which are either all h, k, l even or all h, k, l odd.

2. Since the possible h, k, l reflections in face-centered cubic crystals are known and the distance between planes of this family is given by $a^2/(h^2 + k^2 + l^2)^{1/2}$, the magnitude of the reciprocal space vector which represents each reflection must correspond to this planar distance.

3. The vector magnitudes are obtained from the relative location of the diffraction spots on the film and the ratios of these magnitudes must correspond to the ratios of the interplanar distances of certain possible reflections. This correspondence is found by trial and error using a minimum of three diffraction spots.

4. When the correct ratios are found, the diffraction spots are designated on the film and the pattern is indexed completely by

making use of the fact that the spots must be consistent and in a straight line in reciprocal space.

5. The foil normal is obtained by use of the cross product of any two of the determined directions.

6. The vector representing the line of intersection of any slip plane with the foil surface is obtained from the cross product of the directions representing their normals.

7. The angle that is formed between any two planes in the plane of the foil can be obtained from the dot product of the vectors representing the intersections of the planes and the foil surface.

8. The angle between any two planes can be determined from the dot product of their normals.

BIBLIOGRAPHY

1. D. H. Avery and W. A. Backoffen, "Fatigue Hardening in Alloys of Low Stacking-Faulty Energy," Acta Met., II, (1963), 653.

2. J. E. Bailey and P. B. Hirsch, "The Dislocation Distribution, Flow Stress and Stored Energy in Cold Worked Polycrystalline Silver," Phil. Mag., 5, (1960), 485.

3. J. E. Bailey, "The Dislocation Density,Flow Stress and Stored Energy in Deformed Polycrystalline Copper," Phil. Mag., 8, (1963), 223.

4. H. M. Bendler, "Origins of Electron Interference Effects in Thin Crystals," Internal Stresses and Fatigue in Metals, Elsevier London, (1959), 120.

5. H. M. Bendler and W. A. Wood, "Effect of Superimposed Static Tension on the Fatigue Process in Copper Subjected to Alternating Torsion," Research Laboratories, General Motors Corporation, Warren, Michigan, (1961).

6. H. M. Bendler and W. A. Wood, "The Fatigue Process in Copper as Studied by Electron Metallography," Research Laboratories, General Motors Corporation, Warren, Michigan (1961).

7. H. M. Bendler and W. A. Wood, "Electron Metallographic Observations on the Formation of Fatigue Cracks," Acta Met., 8, (1960), 402.

8. W. C. Bigelow, "The Development of Electron Microscopic Methods for the Study of Metals," ASTM, STP, 317, (1962), 58.

9. W. Bollman, "Interference Effects in Electron Microscopy of Thin Crystals," Phys. Rev., 103, (1956), 1588.

10. A. H. Cottrell and D. Hull, "Extrusion and Intrusion by Cyclic Slip in Copper," Proc. Roy. Soc., A242, (1957), 211.

11. J. A. Ewing and J. W. C. Humfrey, "The Fracture of Metals Under Repeated Alternations of Stress," Phil. Trans., Roy. Soc., (London) A200, (1903), 241.

12. C. E. Feltner, "Dislocation Arrangements in Aluminum Deformed by Repeated Tensile Stresses," Acta. Met., II, (1963), 817.

13. R. M. Fisher and A. Szirmae, "Observations of Dislocations in Thin Foils of Stainless Steel with the Electron Microscope," ASTM, STP, 262, (1959), 103.

14. P. J. E. Forsyth, "Some Observations on the Nature of Fatigue Damage," Phil. Mag., 2, (1957), 437.

15. P. J. E. Forsyth, Fatigue in Aircraft Structures, A.M. Freudenthal Ed., New York, Academic Press, (1956).

16. P. J. E. Forsyth, "Fatigue Crack Formation in Silver Chloride," ASTM, STP, 237, (1958), 21.

17. J. T. Fourie and H. G. F. Wilsdorf, "Production of Dislocation Loops by a Combined Climb and Glide Mechanism," J. Appl. Phys., 31, (1960), 2219.

18. H. J. Gough, "Crystalline Structure in Relation to Failure of Metals, Especially by Fatigue," Proc. ASTM, 33, II, (1933), 3.

19. H. J. Gough, "Behavior of a Single Crystal of Alpha Iron Subjected to Alternating Torsional Stresses," Proc. Rev. Soc., A118, (1928), 498.

20. H. J. Gough, Fatigue of Metals, Ben, London, (1924).

21. H. J. Gough and D. G. Sopwith, "Atmospheric Action as a Factor in Fatigue," J. Inst. Met., 49, (1932), 93.

22. H. J. Gough and D. G. Sopwith, "Some Further Experiments on Atmospheric Action in Fatigue," J. Inst. Met., 56, (1935).

23. H. J. Gough and D. G. Sopwith, "Inert Atmospheres as Fatigue Environments," J. Inst. Met., 72, (1946), 415.

24. J. C. Grosskreutz, "The Formation of Substructure in Aluminum During Alternating Plastic Strain," J. Appl. Phys., 34, (1962), 372.

25. J. C. Grosskreutz, "The Formation of Substructure in Aluminum During Alternating Plastic Strain," Fifth International Congress for Electron Microscopy, Academic Press, I, (1962), J-9.

26. J. C. Grosskreutz and P. Waldow, "Substructure and Fatigue Fracture in Aluminum," Acta Met., 2, (1963), 717.

27. M. Hempel, "Performance of Steel Under Repeated Loading," Fatigue in Aircraft Structures, New York, Academic Press, (1956), 83.

28. M. Hempel, "Slipband Formation and Fatigue Cracks Under Alternating Stress," ASTM, STP, 237, (1958), 52.

29. R. D. Hiedenreich, "Electron Microscope and Diffraction Study to Metal Crystal Textures by Means of Thin Sections," J. Appl. Phys., 20, (1949), 993.

30. P. B. Hirsch, "Observations of Dislocations in Metals," Internal Stresses and Fatigue in Metals, Elsevier, London, (1960).

31. P. B. Hirsch, "Observations of Dislocations in Metals by Transmission Electron Microscopy," J. Inst. Met., 87, (1959), 406.

32. P. B. Hirsch, A. Howie and M. J. Whelan, "A Kinematical Theory of Diffraction Contrast of Electron Transmission Microscope Images of Dislocations and Other Defects," Proc. Roy. Soc., 252, (1960),

33. P. B. Hirsch, P. G. Partridge and R. L. Segall, "An Electron Microscope Study of Stainless Steel Deformed in Fatigue and Simple Tension," Phil. Mag., 4, (1959), 721.

34. J. P. Hirth, "Dislocation Interactions in the Face-centred Cubic Lattice," J. Appl. Phys., 31, (1961), 701.

35. J. Holden, "The Formation of Subgrain Structure by Alternating Plastic Strain," Phil. Mag., 6, (1961), 547.

36. J. Holden, "Observations of Cyclic Structure at Large Ranges of Plastic Strain," Acta. Met., II, 7, (1963), 691.

37. A. Howie, "Dislocation Arrangements In Deformed Face-centred Cubic Single Crystals of Different Stacking Fault Energy," Imperfections In Solids, Interscience Pub., New York, (1961).

38. A. Howie, "Interpretations of Transmission Electron Microscope Images of Dislocations and Stacking Faults," Imperfections in Solids, Interscience Pub., New York, (1961).

39. D. Kay, Techniques for Electron Microscopy, Charles C. Thomas, Illinois, (1961).

40. P. M. Kelly and J. Nutting, "Techniques for the Direct Examination of Metals by Transmission in the Electron Microscope," J. Inst. Met., 87, (1959), 385.

41. D. S. Kemsley, "Behavior of Fractured Copper Fatigue Specimens on Annealing," J. Inst. Met., 85, (1957), 417.

42. D. S. Kemsley, "Effects of Cyclic Stress and Frequency on Deformation Markings in Fatigued Copper," J. Inst. Met., 85, (1957), 420.

43. D. S. Kemsley, and M. S. Paterson, "The Influence of Strain Amplitide on the Work Hardening of Copper Crystals in Alternating Tension and Compression," Acta. Met., 8, (1960), 453.

44. F. N. Mott, "A Theory of the Origin of Fatigue Cracks," Acta Met., 6, (1958), 195.

45. Z. G. Pinsker, Electron Diffraction, Butterworths Scientific Publications, London, (1953).

46. Product Engineering, (Nov. 12, 1962), 69.

47. W. T. Read, Dislocations in Crystals, McGraw Hill, New York, (1953).

48. R. L. Segall, P. G. Partridge and P. B. Hirsch, "The Dislocation Distribution in Face-centred Cubic Metals After Fatigue," Phil. Mag., 6, (1961), 1493.

49. R. L. Segall and P. G. Partridge, "Dislocation Arrangements in Aluminum Deformed in Tension or by Fatigue," Phil. Mag., 4, (1959), 912.

50. K. U. Snowden, "Dislocation Arrangements During Cyclic Hardening and Softening in Aluminum Crystals," Acta. Met., II, (1963), 675.

51. K. U. Snowden, "The Bauschinger Effect and Dislocation Arrangements in Aluminum Single Crystals Deformed by Cyclic Straining," Fifth International Congress for Electron Microscopy," I, (1962), J-7.

52. P. R. Strutt, "Preparation of Thin Metal Foils from Ordinary Tensile Specimens for Use in Transmission Electron Microscopy," Review of Scientific Instruments, 23, (1961), 4, 411.

53. P. R. Swann and J. Nutting, "Stacking Faults and the Failure of Alloys in Corrosive Media," J. Inst. Met., 88, (1960), 478.

54. A. Szirmae and R. N. Fisher, A.S.T.M. Conference, (June 1963) To Be Published.

55. G. Thomas, Transmission Electron Microscopy of Metals, John Wiley and Sons, Inc., (1962).

56. K. Thomas, "Electron Microscope Investigation of Fatigue," Fifth International Congress for Electron Microscopy, Academic Press, I, (1962), J-6.

57. K. Thomas and K. F. Hale, "The Direct Observation of Metalic Surfaces in the Electron Microscope," Phil. Mag., 4, (1959), 531.

58. Van Norman Thompson, "Metal Fatigue," Zeit.f. Metallkde, Vol. 53, (1962), 71.

59. N. Thompson, "Experiments Relating to the Origin of Fatigue Cracks," Fatigue in Aircraft Structures, Academic Press Inc., New York, N.Y., (1956).

60. H. M. Tomlinson, "An Electropolishing Technique for the Preparation of Metal Specimens for Transmission Electron Microscopy," Phil. Mag., 3, (1958), 867.

61. U. Valdré, "Rearrangement of Dislocations in Stainless Steel During Electropolishing," Fifth International Congress for Electron Microscopy, Academic Press, I, CC-15, (1962).

62. U. Valdré and P. B. Hirsch, "Rearrangements of Dislocations in Stainless Steel During Electropolishing," Phil. Mag., 8, (1963), 237.

63. R. Vandervoort and J. Washburn, "On the Stability of Dislocation Substructure in Quenched Aluminum," Phil. Mag., 5, (1960), 24.

64. N. J. Wadsworth and J. Hutchings, "The Effect of Atmospheric Corrosion on Metal Fatigue," Phil. Mag., 3, (1958), 1154.

65. M. J. Whelan, "Dislocation Interactions in Face-Centred Cubic Metals, with Particular Reference to Stainless Steel," Proc. Rev. Soc. (London), 249, (1959), 114.

66. M. J. Whelan, "An Outline of the Theory of Diffraction Contrast Observed at Dislocations and Other Defects in Thin Crystals Examined by Transmission Electron Microscopy," J. Inst. Met., 87, (1959), 406.

67. M. J. Whelan, P. B. Hirsch and R. W. Horne, "Dislocations and Stacking Faults in Stainless Steel," Proc. Roy. Soc., (London), 240, (1959), 524.

68. Doris Kuhlmann-Wilsdorf, "Frictional Stress Acting on a Moving Dislocation in an Otherwise Perfect Crystal," Phys. Rev., 120, (1960), 3.

69. H. G. F. Wilsdorf, "The Role of Transmission Electron Microscopy in Fundamental Fatigue Studies," Materials Research and Standards, 640, (1962).

70. H. G. F. Wilsdorf and D. Kuhlmann-Wilsdorf, "Dislocation Behavior in Quenched and in Neutron Irradiated Stainless Steel," J. Nucl. Mat., 5, (1962), 178.

71. H. G. F. Wilsdorf and D. Kulhmann-Wilsdorf, "Considerations of Interactions Between Thermal Vacancies and Dislocations, Phys. Rev. Letters, 3, (1959), 170.

72. H. G. F. Wilsdorf and D. Kuhlmann-Wilsdorf, "Production of Point Defects and Jogs Through Dislocation Uncertainty," Acta. Met., 10, (1962), 5, 584.

73. D. Kuhlmann-Wilsdorf, R. Maddin and H. G. F. Wilsdorf, "Point Defect Hardening in Face-Centred Cubic Metals," Strengthening Mechanisms in Solids, ASM, (1960), 137.

74. H. G. F. Wilsdorf, "Dislocation Patterns in Deformed Alpha-Brass," Internal Stresses and Fatigue in Metals, Elsevier, London, (1959), 178.

75. H. G. F. Wilsdorf and J. Schmitz, "The Observation of Dislocation Tangles in the Easy Glide Range of Aluminum," J. Appl. Phys., 33, (1962), 5, 1750.

76. R. N. Wilson and P. J. E. Forsyth, "Some New Observations on Fatigue Damage," J. Inst. Met., 87, (1959), 336.

77. W. A. Wood, "Formation of Fatigue Cracks," Phil. Mag., 3, (1958), 692.

78. W. A. Wood, Fatigue in Aircraft Structures, Academic Press, N.Y., (1956).

79. W. A. Wood, "Recent Observations in Fatigue Failure in Metals," ASTM, STP, 237, (1958), 110.

80. W. A. Wood, S. McK. Cousland and K. R. Sargant, "Systematic Microstructural Changes Peculiar to Fatigue Deformation," Acta. Met., II, (1963), 7, 643.